

Graphical Abstract

A model for pipes conveying fluid considering bending-axial-torsional dynamics and their interconnected effects on stability

Vitor Schwenck Franco Maciel, Guilherme Vernizzi, Mojtaba Kheiri, Guilherme Rosa Franzini

Highlights

A model for pipes conveying fluid considering bending-axial-torsional dynamics and their interconnected effects on stability

Vitor Schwenck Franco Maciel, Guilherme Vernizzi, Mojtaba Kheiri, Guilherme Rosa Franzini



A model for pipes conveying fluid considering bending-axial-torsional dynamics and their interconnected effects on stability

Vitor Schwenck Franco Maciel^a, Guilherme Vernizzi^a, Mojtaba Kheiri^b,
Guilherme Rosa Franzini^a

^a*Offshore Mechanics Laboratory, Escola Politecnica, University of Sao Paulo, Brazil,*

^b*Fluid-Structure Interactions & Aeroelasticity Laboratory, Concordia University,
Canada,*

Abstract

The present work aims to contribute to the ever growing literature on the topic of modeling internal-flow-induced vibrations in pipes conveying fluid. A three-dimensional and nonlinear mathematical model for a pipe conveying fluid, which includes the axial and torsional dynamics, is comprehensively derived and presented. Nonlinearities up to cubic order are retained in the equations of motion and the dynamics of the pipe is formulated around the axial and torsional static solutions. The effects of applied torsional moments on the stability conditions of the pipe are characterized as a function of their magnitude and attachment position. It is shown that a torsional moment may induce static instabilities in the pipe if above a certain critical value, which is characterized as a function of the point at which it is attached to. Regardless of the magnitude of the torsional moment, it always reduces the critical flow velocities related to the onset of flutter, which may have important practical consequences. While the stability of pipes conveying air is shown to be more sensitive to torsional moments applied at its free end, for pipes conveying water, middle point applications are more severe. Depending on the parameters of the system, divergence and flutter may either coexist, or the system is stabilized by internal flow velocities smaller than the ones related to the onset of flutter. By numerically integrating the equations of motion, it is also shown that the presence of torsional moments induce three-dimensional motions on the pipe, even when two-dimensional initial conditions are given.

Keywords: Fluid-structure interactions, Pipes conveying fluid, Internal-flow-induced vibrations in pipes

1. Introduction

The reasons for the increasing interest in the study of pipes conveying fluid are many. Firstly, it is a physically simple manifestation of fluid-structure interactions (FSI) and can be observed, for instance, in something as mundane as a garden hose. Consequently, assembling experimental arrangements can be relatively simple when compared to other FSI phenomena. Secondly, even when mathematical models are derived in a fairly simple manner, the dynamical features exhibited by pipes conveying fluid are rich and often unexpected. These reasons led to this particular problem being justifiably deemed a *model dynamical problem* by the authors in [1]. Along the past decades, a plethora of works comprised of linear and nonlinear analyses have been published on the dynamics of such systems. While curiosity was mostly the main motivation for the early studies on the topic, many practical applications have arisen since then. For example, pipes have become essential components in ocean mining procedures, water supply networks, offshore and deep-water oil and gas production, cave salt mining and, recently, the injection and storing of carbon dioxide within submarine or underground caverns ([2]). For these reasons, the literature on the topic reveals that the complexity with which mathematical models for pipes conveying fluid have been derived has generally increased with time. This increasing complexity may be observed in the seemingly countless modifications considered in these systems, as well as in how the internal flow is modeled. How the pipe itself is modeled, as a structural element, is yet another aspect in which this increasing complexity can be seen. This latter aspect is the focus of the works hereby mentioned.

A theoretical investigation on the dynamics and stability of a system composed of articulated rigid pipes was made in [3]. While simpler than its continuous counterparts, the inherently discrete system studied by Benjamin was shown to display the dynamical instabilities observed when cantilevered pipes convey fluid at postcritical internal flow velocities. Since pipes conveying fluid belong to a wider class of systems whose constituent particles change with time, commonly referred to as *open* systems, the author derived modified versions of the Hamilton's principle and of the Euler-Lagrange equations capable of including the system under study. For additional discussions

regarding appropriate variational principles for open systems, the reader is referred to [4], [5] and, with more focus on the modeling of pipes, [6].

Benjamin's work was extended in [7], where the linear equations of motion (EOM) for a horizontal, inextensible and continuous pipe were derived. The authors showed that, under these conditions, pipes conveying fluid can only lose stability by flutter when conveying fluid at postcritical internal flow velocities. Gravitational effects were included in [8], where it was shown that "hanging" pipes (i.e. pipes discharging fluid in the same direction as the one from the gravitational acceleration) behave very similarly as horizontal ones, albeit with larger critical flow velocities due to the gravitational restoring force. Pipes discharging fluid in the opposite direction as gravity (i.e. "standing" pipes), in turn, were shown to have a more intricate dynamics. More specifically, depending on the parameters characterizing the system, divergence due to its own weight may occur. Also depending on the system parameters, increasing the internal flow velocity was shown to have two qualitatively different effects. In the first one, divergence and flutter were shown to coexist, while in the second, the system was "stabilized by flow" at a flow velocity lower than the one related to the onset of flutter.

One of the many advantages of geometrically nonlinear mathematical models for pipes is their capacity to reproduce the limit-cycle oscillations observed experimentally when the flow velocity is above the critical level. A systematic comparison between the existing nonlinear models up to 1993 was carried out in [9], where the authors derived their own set of nonlinear EOM for a two-dimensional (2D) and inextensible pipe conveying fluid. An additional displacement field was included in [10], where a 2D extensible pipe was considered and the EOM were derived using the Euler-Lagrange equations for *open* systems published in [11]. The authors showed that the difference between the stability conditions of inextensible and extensible pipes was qualitative, and that the critical flow velocities for extensible pipes were shown to be slightly larger. In [12], although the pipe was considered to be inextensible, the possibility of three-dimensional (3D) motions was included in the mathematical model. Using the model derived in [12], the authors in [13] showed that the motions of the pipe, in the steady state regime, could be 2D or 3D depending on the parameters of the system. Both these additional displacement fields were included in [14], where a 3D mathematical model for an extensible pipe was presented.

A few additional strategies for modeling pipes conveying fluid are now mentioned. The authors in [15] revisited the derivations made in [9] and, by

relaxing the hypotheses related to finite displacements of the pipe, presented a set of geometrically exact EOM for a 2D and inextensible pipe conveying fluid. Further details on works using similar strategies can be found in [16] and [17]. In [18], in turn, the authors use a modular methodology, which differs from classical approaches in the field by defining the compatibility conditions and non-linearities as mathematical constraints to be enforced during the integration process. This allows the obtaining of a geometrically exact model with a small amount of algebraic work, with the drawback that it does not furnish a set of EOM to be investigated. The reader interested in works focusing on different alternatives for the construction of reduced-order models (ROMs) for pipes conveying fluid is referred to [19], which discuss the use of the proper orthogonal decomposition method, for this purpose, and [20] and [21], in which subspectral submanifolds are used instead. Finally, the extensive review [22] of studies on the topic, published before 2014, is mentioned.

The main goal of the present work is to further contribute to the topic by presenting the derivation of a more *complete* nonlinear mathematical model for a pipe conveying fluid, in terms of the included displacement fields. The present model includes the possibility of 3D motions of the pipe, as well as its axial and torsional dynamics. To the best of the authors' knowledge, the role played by torsion on the dynamics of pipes conveying fluid has not yet been characterized. In addition, with the increasing number of practical applications involving pipes conveying fluid, localized torsional moments may be applied at a point along the pipe. The second objective of the present work is to characterize the effects that such moments may have on the stability conditions of the pipe, depending on its magnitude and attachment position.

The rest of this paper is organized as follows. Section 2 contains the derivation of the mathematical model, while Sec. 3 gathers important methodological aspects with which the mathematical model is investigated. While the main results are shown and discussed in Sec. 4, Sec. 5 is dedicated to summarizing the main conclusions drawn from the present work.

2. Mathematical Model

This section is dedicated to the derivation of the present mathematical model. Initially, in Subsec. 2.1, the system is described and the main hypotheses adopted, gathered. The kinematic description of the configuration of the pipe is made using Euler angles, which are defined in Subsec. 2.2.

Then, Subsec. 2.3 addresses the definition of the displacements and derivation of the strain measures for generic points belonging to the pipe. Also contained in Subsec. 2.3 is the derivation of the nonlinear generalized curvature expressions used in the derivation of the EOM, which is detailed in Subsec. 2.4.

2.1. Description of the system and main hypotheses

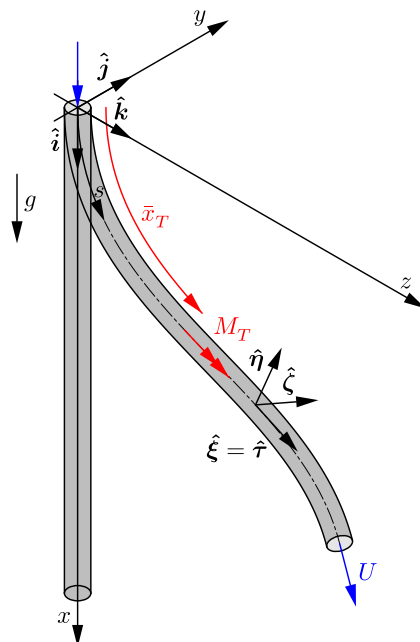


Figure 1: Schematic drawing of a hanging pipe conveying fluid shown in both initial and deflected configurations. The fluid enters through the clamped end of the pipe and is discharged through its free end. While (x, y, z) is a global fixed coordinate system, (ξ, η, ζ) is a local reference frame. A localized torsional moment of magnitude M_T is applied at a point \bar{x}_T along the length of the pipe.

Consider the system composed of a hanging cantilevered flexible pipe discharging fluid, as shown in Fig. 1. The pipe has length L , external diameter D , Young's modulus E and shear modulus G . The material of the pipe has density ρ , while the conveyed fluid has specific mass ρ_F and flows at a constant velocity U with respect to the pipe, being discharged to the atmosphere. Denoting by A and A_F the total and internal areas of each cross section, respectively, the masses per unit length of the pipe and fluid

are $m = \rho A$ and $M = \rho_F A_F$, also respectively. A localized torsional moment of magnitude M_T is applied at a point \bar{x}_T along the length of the pipe. While (x, y, z) is a global fixed coordinate system, (ξ, η, ζ) is a local reference frame, as also shown in Fig. 1. Denoted by I_y and I_z are the moments of inertia with respect to the y - and z -axes, respectively. Additionally, I_p and I_4 are the polar moment of inertia and fourth-order polar moment, respectively. The pipe has a vertical position in its undeflected configuration and the gravitational acceleration is given by $\mathbf{g} = g\hat{\mathbf{i}}$, where a “standing” pipe can be investigated by simply using a negative value for g (see [8]).

It is assumed that the material of the pipe has a linear-elastic constitutive behavior and that its properties (ρ, D, A, A_F, E, G) are constant along its length. The plug-flow model is adopted – the fluid is considered as incompressible and its velocity profile, as uniform inside the pipe. The pipe is assumed to behave as a Kirchhoff beam and, given that the cross sections are circular and are expected to possess thin walls, no warping is considered. Consequently, the cross sections are assumed to behave as rigid bodies and, in addition, their rotary inertia is neglected. Both transverse and torsional displacements are assumed to be one order larger ($\mathcal{O}(\varepsilon)$) than the axial displacements ($\mathcal{O}(\varepsilon^2)$). While large displacements are considered in the mathematical model (nonlinearities up to $\mathcal{O}(\varepsilon^3)$ in the EOM), the strains are assumed to be small, which is due to the adopted rheological model for the pipe material. The structural modeling for the pipe as a Kirchhoff beam able to experience flexure along two principal directions, as well as extension and torsion is made following the work published in [23].

2.2. Definition of the Euler angles

The Euler Angles are defined as follows: firstly, a rotation θ_y is given around the y -axis, leading to the (ξ_1, η_1, ζ_1) coordinate system (see Fig. 2 (a)); secondly, a rotation θ_z is given around the ζ_1 -axis, leading to the (ξ_2, η_2, ζ_2) coordinate system (see Fig. 2 (b)); lastly, a rotation θ_x around the ξ_2 -axis leads to the (ξ, η, ζ) coordinate system (see Fig. 2 (c)). The last rotation given θ_x is associated with the torsional displacements.

From Figs. 2, the direct relations between the (x, y, z) and (ξ, η, ζ) coordinate systems can be written as

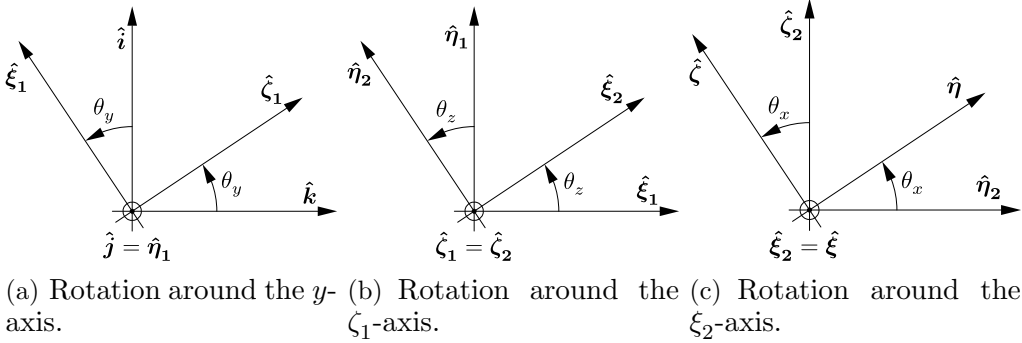


Figure 2: Definition of the Euler Angles.

$$\begin{aligned}
\hat{\mathbf{i}} &= i_\xi \hat{\boldsymbol{\xi}} + i_\eta \hat{\boldsymbol{\eta}} + i_\zeta \hat{\boldsymbol{\zeta}}, \text{ where } \begin{cases} i_\xi = \cos \theta_y \cos \theta_z \\ i_\eta = \sin \theta_y \sin \theta_z - \cos \theta_y \sin \theta_z \cos \theta_x \\ i_\zeta = \sin \theta_y \cos \theta_x + \cos \theta_y \sin \theta_z \sin \theta_x \end{cases}, \\
\hat{\mathbf{j}} &= j_\xi \hat{\boldsymbol{\xi}} + j_\eta \hat{\boldsymbol{\eta}} + j_\zeta \hat{\boldsymbol{\zeta}}, \text{ where } \begin{cases} j_\xi = \sin \theta_z \\ j_\eta = \cos \theta_z \cos \theta_x \\ j_\zeta = -\cos \theta_z \sin \theta_x \end{cases}, \text{ and} \\
\hat{\mathbf{k}} &= k_\xi \hat{\boldsymbol{\xi}} + k_\eta \hat{\boldsymbol{\eta}} + k_\zeta \hat{\boldsymbol{\zeta}}, \text{ where } \begin{cases} k_\xi = -\sin \theta_y \cos \theta_z \\ k_\eta = \cos \theta_y \sin \theta_z + \sin \theta_y \sin \theta_z \cos \theta_x \\ k_\zeta = \cos \theta_y \cos \theta_x - \sin \theta_y \sin \theta_z \sin \theta_x \end{cases}.
\end{aligned} \tag{1}$$

2.3. Displacements and strain measures

Consider two contiguous points P_0 and Q_0 which belong to the centreline of the pipe and are at $(x_{P_0}, 0, 0)$ and $(x_{Q_0}, 0, 0)$ in the undeflected configuration, respectively. As the pipe deflects, these points become P and Q and move to the position (x_P, y_P, z_P) and (x_Q, y_Q, z_Q) , respectively. The displacements u, v and w are defined as

$$u_{P,Q} = x_{P,Q} - x_{P_0,Q_0}, \quad v_{P,Q} = y_{P,Q} - y_{P_0,Q_0}, \quad \text{and} \quad w_{P,Q} = z_{P,Q} - z_{P_0,Q_0}. \tag{2}$$

The geometrical description given above is shown in Fig. 3.

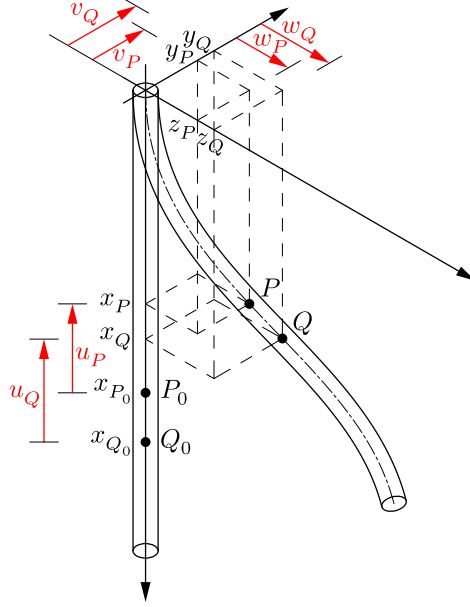


Figure 3: Sketch defining the displacements in each axis: two contiguous points P_0 and Q_0 belong to the centreline of the pipe and are at $(x_{P_0}, 0, 0)$ and $(x_{Q_0}, 0, 0)$ in the undeflected configuration, respectively. As the pipe deflects, these points become P and Q and move to the positions (x_P, y_P, z_P) and (x_Q, y_Q, z_Q) , respectively.

2.3.1. Strain measures of the centreline

The quadratic strain of the centreline of the pipe can be evaluated by, using Eqs. (2) to write it in terms of the displacements u , v and w ,

$$\begin{aligned} \varepsilon_q &= \frac{1}{2} \left(\frac{\|PQ\|^2 - \|P_0Q_0\|^2}{\|P_0Q_0\|^2} \right) = \\ &= \frac{1}{2} \left(2 \frac{(u_Q - u_P)}{(x_{Q_0} - x_{P_0})} + \frac{(u_Q - u_P)^2}{(x_{Q_0} - x_{P_0})^2} + \frac{(v_Q - v_P)^2}{(x_{Q_0} - x_{P_0})^2} + \frac{(w_Q - w_P)^2}{(x_{Q_0} - x_{P_0})^2} \right). \end{aligned} \quad (3)$$

Considering that P and Q are infinitely close to each other and using the notation $()' = \partial(\)/\partial s_0$, Eq. (3) becomes, gathering terms up to $\mathcal{O}(\varepsilon^3)$,

$$\begin{aligned}\varepsilon_q &= \frac{1}{2} \lim_{ds_0 \rightarrow 0} \left\{ 2 \frac{u(s_0 + ds_0) - u(s_0)}{ds_0} + \frac{[u(s_0 + ds_0) - u(s_0)]^2}{ds_0^2} + \right. \\ &\quad \left. + \frac{[v(s_0 + ds_0) - v(s_0)]^2}{ds_0^2} + \frac{[w(s_0 + ds_0) - w(s_0)]^2}{ds_0^2} \right\} \Rightarrow \\ &\Rightarrow \varepsilon_q = u' + \frac{u'^2 + v'^2 + w'^2}{2} = u' + \frac{v'^2 + w'^2}{2} + \mathcal{O}(\varepsilon^4).\end{aligned}\quad (4)$$

2.3.2. Relations between the Euler angles and the displacements

Having in mind the derivations carried out in Subsubsec. 2.3.3 and in Subsec. 2.4, it is convenient to derive, at this point, relations between the Euler angles θ_y and θ_z and the displacement fields u , v , w and θ_x . Among other alternatives, this can be made using expressions for the tangential vector $\boldsymbol{\tau}$ using the global (x, y, z) and local (ξ, η, ζ) reference frames. This is the procedure used in the present work.

A tangential vector (see Fig. 1) can be obtained from the position vector of a point belonging to the centreline of the pipe by, using Eqs. (2),

$$\boldsymbol{\tau} = \frac{\partial \mathbf{r}}{\partial s_0} = \frac{\partial ((u + x_0)\hat{\mathbf{i}} + v\hat{\mathbf{j}} + w\hat{\mathbf{k}})}{\partial s_0} = (1 + u')\hat{\mathbf{i}} + v'\hat{\mathbf{j}} + w'\hat{\mathbf{k}}.\quad (5)$$

Using the transformations (1) in Eq. (5), this tangential vector can be written in the (ξ, η, ζ) local reference frame as

$$\boldsymbol{\tau} = [(1 + u')i_\xi + v'j_\xi + w'k_\xi]\hat{\boldsymbol{\xi}} + [(1 + u')i_\eta + v'j_\eta + w'k_\eta]\hat{\boldsymbol{\eta}} + [(1 + u')i_\zeta + v'j_\zeta + w'k_\zeta]\hat{\boldsymbol{\zeta}} = a\hat{\boldsymbol{\xi}} + 0\hat{\boldsymbol{\eta}} + 0\hat{\boldsymbol{\zeta}}, \text{ where } a \in \mathbb{R}.\quad (6)$$

Equating either the $\hat{\boldsymbol{\eta}}$ or $\hat{\boldsymbol{\zeta}}$ components on the right and left hand side of Eq. (6) leads to

$$\begin{aligned}\{[w' \sin \theta_y - (1 + u') \cos \theta_y] + v' \cos \theta_z\} \cos \theta_x + \\ + [(1 + u') \sin \theta_y + w' \cos \theta_y] \sin \theta_x = 0.\end{aligned}\quad (7)$$

Since Eq. (7) must be true for $\forall \theta_x$ and using the well known trigonometric identity $\tan^2 \theta = \sec^2 \theta - 1$, the following relations are obtained:

$$\begin{cases} \sin \theta_y = -\frac{w'}{\sqrt{w'^2+(1+u')^2}} \\ \cos \theta_y = \frac{1+u'}{\sqrt{w'^2+(1+u')^2}} \\ \tan \theta_y = -\frac{w'}{(1+u')} \end{cases}, \text{ and } \begin{cases} \sin \theta_z = \frac{v'}{\sqrt{v'^2+w'^2+(1+u')^2}} \\ \cos \theta_z = \frac{\sqrt{w'^2+(1+u')^2}}{\sqrt{v'^2+w'^2+(1+u')^2}} \\ \tan \theta_z = \frac{v'}{\sqrt{w'^2+(1+u')^2}} \end{cases}. \quad (8)$$

A substitution of Eqs. (8) into the transformations (1) allows for them to be written in terms of the displacements u, v, w and θ_x as

$$\begin{cases} i_\xi = \frac{1+u'}{\sqrt{v'^2+w'^2+(1+u')^2}} \\ i_\eta = -\left(\frac{w'}{\sqrt{w'^2+(1+u')^2}}\right) \sin \theta_x - \left(\frac{1+u'}{\sqrt{w'^2+(1+u')^2}}\right) \left(\frac{v'}{\sqrt{v'^2+w'^2+(1+u')^2}}\right) \cos \theta_x \\ i_\zeta = -\left(\frac{w'}{\sqrt{w'^2+(1+u')^2}}\right) \cos \theta_x + \left(\frac{1+u'}{\sqrt{w'^2+(1+u')^2}}\right) \left(\frac{v'}{\sqrt{v'^2+w'^2+(1+u')^2}}\right) \sin \theta_x \end{cases},$$

$$\begin{cases} j_\xi = \frac{v'}{\sqrt{v'^2+w'^2+(1+u')^2}} \\ j_\eta = \left(\frac{\sqrt{w'^2+(1+u')^2}}{\sqrt{v'^2+w'^2+(1+u')^2}}\right) \cos \theta_x \\ j_\zeta = -\left(\frac{\sqrt{w'^2+(1+u')^2}}{\sqrt{v'^2+w'^2+(1+u')^2}}\right) \sin \theta_x \end{cases}, \text{ and}$$

$$\begin{cases} k_\xi = \frac{w'}{\sqrt{v'^2+w'^2+(1+u')^2}} \\ k_\eta = \left(\frac{1+u'}{\sqrt{w'^2+(1+u')^2}}\right) \sin \theta_x - \left(\frac{w'}{\sqrt{w'^2+(1+u')^2}}\right) \left(\frac{v'}{\sqrt{v'^2+w'^2+(1+u')^2}}\right) \cos \theta_x \\ k_\zeta = \left(\frac{1+u'}{\sqrt{w'^2+(1+u')^2}}\right) \cos \theta_x + \left(\frac{w'}{\sqrt{w'^2+(1+u')^2}}\right) \left(\frac{v'}{\sqrt{v'^2+w'^2+(1+u')^2}}\right) \sin \theta_x \end{cases}.$$
(9)

At this point, Eqs. (8) and (9) are geometrically exact.

2.3.3. Strain measures for a generic point of the pipe and nonlinear generalized curvature expressions

The strain measures for a generic point of the pipe are determined using the Green strain tensor

$$\mathbf{E} = \begin{bmatrix} \varepsilon_{\xi\xi} & \varepsilon_{\xi\eta} & \varepsilon_{\xi\zeta} \\ \varepsilon_{\eta\xi} & \varepsilon_{\eta\eta} & \varepsilon_{\eta\zeta} \\ \varepsilon_{\zeta\xi} & \varepsilon_{\zeta\eta} & \varepsilon_{\zeta\zeta} \end{bmatrix}, \text{ such that} \quad (10)$$

$$d\mathbf{r}_R \cdot d\mathbf{r}_R - d\mathbf{r}_{R_0} \cdot d\mathbf{r}_{R_0} = 2d\mathbf{r}_{R_0}^T \mathbf{E} d\mathbf{r}_{R_0}, \quad (11)$$

where $d\mathbf{r}_R$ and $d\mathbf{r}_{R_0}$ are the differential position vectors of a generic point R in the deflected and undeflected configuration of the pipe, respectively.

Considering that R belongs to the same cross section as P and with coordinates $y_R \hat{\boldsymbol{\eta}} + z_R \hat{\boldsymbol{\zeta}}$, relative to P (see Fig. 4), its position vectors \mathbf{r}_R and \mathbf{r}_{R_0} can be written as

$$\begin{aligned} \mathbf{r}_{R_0} &= x \hat{\mathbf{i}} + y_{R_0} \hat{\mathbf{j}} + z_{R_0} \hat{\mathbf{k}}, \\ \mathbf{r}_R &= (x + u) \hat{\mathbf{i}} + v \hat{\mathbf{j}} + w \hat{\mathbf{k}} + y_R \hat{\boldsymbol{\eta}} + z_R \hat{\boldsymbol{\zeta}}. \end{aligned} \quad (12)$$

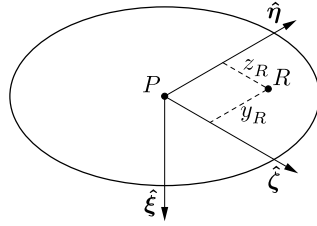


Figure 4: Relative position between a point P , belonging to the centreline of the pipe, and R , which lies in the same cross section as P and with coordinates $y_R \hat{\boldsymbol{\eta}} + z_R \hat{\boldsymbol{\zeta}}$ relative to it.

Differentiating \mathbf{r}_R with respect to s_0 leads to

$$d\mathbf{r}_R = (1 + u')ds \hat{\mathbf{i}} + v'ds \hat{\mathbf{j}} + w'ds \hat{\mathbf{k}} + dy_R \hat{\boldsymbol{\eta}} + dz_R \hat{\boldsymbol{\zeta}} + \mathbf{C} \times (y_R \hat{\boldsymbol{\eta}} + z_R \hat{\boldsymbol{\zeta}})ds, \quad (13)$$

where $\mathbf{C} = \theta'_x \hat{\boldsymbol{\xi}} + \theta'_y \hat{\boldsymbol{\eta}}_1 + \theta'_z \hat{\boldsymbol{\zeta}}_2$ is the “spatial angular velocity” vector, or the generalized curvature vector of the pipe. When written in the (ξ, η, ζ) local reference frame, the expression for \mathbf{C} becomes

$$\mathbf{C} = C_\xi \hat{\boldsymbol{\xi}} + C_\eta \hat{\boldsymbol{\eta}} + C_\zeta \hat{\boldsymbol{\zeta}}, \text{ where } \begin{cases} C_\xi = \theta'_x + \theta'_y \sin \theta_z \\ C_\eta = \theta'_y \cos \theta_z \cos \theta_x + \theta'_z \sin \theta_x \\ C_\zeta = -\theta'_y \cos \theta_z \sin \theta_x + \theta'_z \cos \theta_x \end{cases}. \quad (14)$$

By substituting the transformations (1) and Eq. (14) into Eqs. (13), $d\mathbf{r}_R$ can be written as

$$\begin{aligned} d\mathbf{r}_R = & [(1+u')ds i_\xi + v'ds j_\xi + w'ds k_\xi + C_\eta z_R ds - C_\zeta y_R ds] \hat{\boldsymbol{\xi}} + \\ & + [(1+u')ds i_\eta + v'ds j_\eta + w'ds k_\eta + dy_R - C_\xi z_R ds] \hat{\boldsymbol{\eta}} + \\ & + [(1+u')ds i_\zeta + v'ds j_\zeta + w'ds k_\zeta + dz_R + C_\xi y_R ds] \hat{\boldsymbol{\zeta}}. \end{aligned} \quad (15)$$

Using the facts that $\|\hat{\mathbf{i}}\|^2 = \|\hat{\mathbf{j}}\|^2 = \|\hat{\mathbf{k}}\|^2 = 1$ and that $\hat{\mathbf{i}}$, $\hat{\mathbf{j}}$ and $\hat{\mathbf{k}}$ are orthogonal to each other, as well as Eqs. (9), the scalar product $d\mathbf{r}_R \cdot d\mathbf{r}_R$ can be written as, after many algebraic manipulations,

$$\begin{aligned} d\mathbf{r}_R \cdot d\mathbf{r}_R = & \left[\sqrt{(1+u')^2 + v'^2 + w'^2} ds + (C_\eta z_R - C_\zeta y_R) ds \right]^2 + dy_R^2 + dz_R^2 - \\ & - 2dy_R C_\xi z_R ds + 2dz_R C_\xi y_R ds + (C_\xi z_R ds)^2 + (C_\xi y_R ds)^2. \end{aligned} \quad (16)$$

Defining

$$\varepsilon^* \triangleq \left(\sqrt{(1+u')^2 + v'^2 + w'^2} - 1 \right) + C_\eta z_R - C_\zeta y_R = \varepsilon_\ell + C_\eta z_R - C_\zeta y_R, \quad (17)$$

where $\varepsilon_\ell = \sqrt{2\varepsilon_q + 1} - 1$ is the linear strain measure, the left-hand side of Eq. (11) becomes

$$\begin{aligned} d\mathbf{r}_R \cdot d\mathbf{r}_R - d\mathbf{r}_{R_0} \cdot d\mathbf{r}_{R_0} = & (\varepsilon^* + 1)^2 ds^2 - ds^2 - 2dy_R C_\xi z_R ds + 2dz_R C_\xi y_R ds + \\ & + (C_\xi z_R ds)^2 + (C_\xi y_R ds)^2. \end{aligned} \quad (18)$$

Using the symmetry of \mathbf{E} , the right-hand side of Eq. (11), in turn, is given by

$$\begin{aligned} 2d\mathbf{r}_{R_0}^T \mathbf{E} d\mathbf{r}_{R_0} = & 2\varepsilon_{\xi\xi} ds^2 + 4\varepsilon_{\xi\eta} dy_R ds + 4\varepsilon_{\xi\zeta} dz_R ds + 4\varepsilon_{\eta\zeta} dz_R dy_R + \\ & + 2\varepsilon_{\eta\eta} dy_R^2 + 2\varepsilon_{\zeta\zeta} dz_R^2. \end{aligned} \quad (19)$$

Equating Eqs. (18) and (19) provides the following strain measures:

$$\begin{aligned}\varepsilon_{\xi\xi} &= \frac{(\varepsilon^* + 1)^2 - 1 + (C_\xi z_R)^2 + (C_\xi y_R)^2}{2} \approx \varepsilon^* + \frac{C_\xi^2(z_R^2 + y_R^2)}{2}, \\ \varepsilon_{\xi\eta} &= -\frac{C_\xi z_R}{2}, \quad \varepsilon_{\xi\zeta} = \frac{C_\xi y_R}{2} \text{ and } \varepsilon_{\eta\zeta} = \varepsilon_{\eta\eta} = \varepsilon_{\zeta\zeta} = 0.\end{aligned}\quad (20)$$

where, as mentioned in Subsec. 2.1, the strains are assumed to be small, and thus the expression of $\varepsilon_{\xi\xi}$ is linearized with respect to ε^* . Notice that, while ε^* represents the axial strain for a generic point taking into account the effects of both transversal curvature components C_η and C_ζ , $\varepsilon_{\xi\xi}$ also considers effects of the axial curvature component C_ξ , and thus considers torsional effects. Additionally, the fact that $\varepsilon_{\eta\zeta} = \varepsilon_{\eta\eta} = \varepsilon_{\zeta\zeta} = 0$ is consistent with the assumption that each cross-section behaves as a rigid body.

2.4. Equations of motion

This subsection presents the derivation of the differential EOM which govern the dynamics of the mechanical system described in Sec. 2.1. As already discussed, due to the presence of internal flow inside the pipe, the particles pertaining to the system change with time. This implies in the classification of the system as an “open” system which, in turn, makes the use of the traditional Hamilton’s principle inadequate, in this case. Thus, the generalized Hamilton’s principle for a non-material volume presented in [5] is used instead.

To introduce the variables necessary for said statement, consider two systems, one open and one closed, shown in Figure 5 (a). The closed system can be associated with the control volume $V_c(t)$, which is bounded by the surface $S_c(t)$ and contain a set of particles of density ρ , each with position vector \mathbf{r} and velocity vector \mathbf{u} . Let $V_o(t)$ be the control volume of an open system, bounded by $S_c(t) \cup S_o(t)$, coincident with $V_c(t)$ at time t . Now consider that the portion $S_o(t)$ of the surface of the control volume $V_o(t)$ is able to move with velocity $\mathbf{V} \cdot \mathbf{n}$, where \mathbf{n} is the outward normal to the surface, across which mass can be transported. Figure 5 (b) shows both systems at an instant $t + dt$. For the problem under consideration, $S_c(t)$ can be associated with the surface covered by the pipe wall while $S_o(t)$, to the inlet and outlet open surfaces for the fluid. Finally, let \mathbf{r}_f be the position vector of fictitious particles that coincide with the boundary of $V_o(t)$ (see [24]).

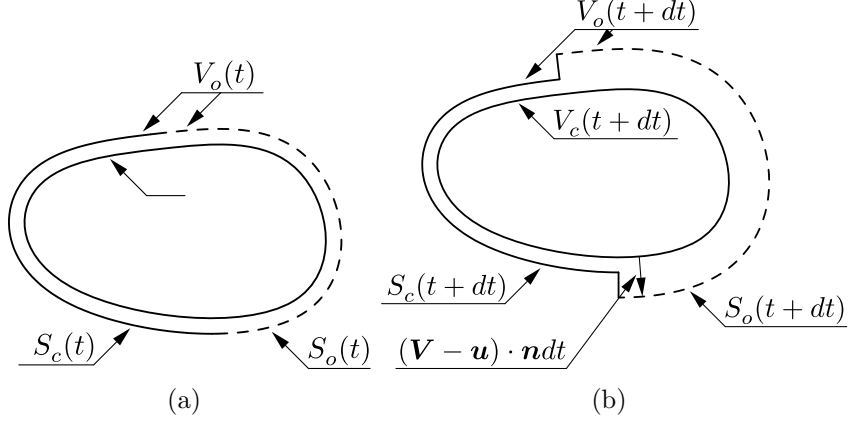


Figure 5: Definition of the control volume of the open system $V_o(t)$. The system is shown at (a) time t ; (b) time $t + dt$. (adapted from [4])

Using the notation $\partial V_o = S_c(t) \cup S_o(t)$ to denote the boundary of the open control volume, the generalized Hamilton's principle states that:

$$\int_{t_1}^{t_2} \left\{ \delta L_o + \delta W - \iint_{\partial V_o} \rho(\mathbf{u} \cdot \delta \mathbf{r})(\mathbf{u} - \mathbf{V}) \cdot \mathbf{n} d\partial V_o + \right. \\ \left. + \iint_{\partial V_o} \frac{1}{2} \rho u^2 (\delta \mathbf{r} - \delta \mathbf{r}_f) \cdot \mathbf{n} d\partial V_o \right\} dt = 0, \quad (21)$$

where $L_o = T_o - V_o$ is the Lagrangean of the open system and δW is the virtual work done by the generalized non-conservative forces. The third term in Eq. (21) represents the flow of momentum while the fourth term represents the flow of kinetic energy across the boundary of the open volume.

The Lagrangean of the open system can be divided into the contributions $L_o = T_o - V_o = (T_p - T_F) + (V_s + V_g)$, where T_p and T_F are the kinetic energies of the pipe and fluid, respectively, and V_g and V_s are the potential energies associated with gravity and strain in the material of the pipe, also respectively.

Firstly, the evaluation of V_s is addressed. As mentioned in Sec. 2.1, the material of the pipe is assumed to stay within the linear elastic rheological model in which the generalized Hooke's law, in the absence of the Poisson

effect, states that $\sigma_{\xi\xi} = E\varepsilon_{\xi\xi}$, $\sigma_{\eta\eta} = E\varepsilon_{\eta\eta}$, $\sigma_{\zeta\zeta} = E\varepsilon_{\zeta\zeta}$, $\sigma_{\xi\eta} = 2G\varepsilon_{\xi\eta}$, $\sigma_{\xi\zeta} = 2G\varepsilon_{\xi\zeta}$ and $\sigma_{\zeta\eta} = 2G\varepsilon_{\zeta\eta}$. Accordingly, the strain energy density function is then given by

$$\begin{aligned} v_s &= \frac{1}{2}(\sigma_{\xi\xi}\varepsilon_{\xi\xi} + \sigma_{\eta\eta}\varepsilon_{\eta\eta} + \sigma_{\zeta\zeta}\varepsilon_{\zeta\zeta} + 2\sigma_{\xi\eta}\varepsilon_{\xi\eta} + 2\sigma_{\xi\zeta}\varepsilon_{\xi\zeta} + 2\sigma_{\zeta\eta}\varepsilon_{\zeta\eta}) = \\ &= \frac{1}{2}E\varepsilon_{\xi\xi}^2 + 2G(\varepsilon_{\xi\eta}^2 + \varepsilon_{\xi\zeta}^2). \end{aligned} \quad (22)$$

Defining V as the total volume of the pipe, the variation of the total strain potential energy stored in the pipe can be evaluated as

$$\delta V_s = \iiint_V \delta v_s \, dV = \iiint_V [E\varepsilon_{\xi\xi}\delta\varepsilon_{\xi\xi} + 4G(\varepsilon_{\xi\eta}\delta\varepsilon_{\xi\eta} + \varepsilon_{\xi\zeta}\delta\varepsilon_{\xi\zeta})] \, dV. \quad (23)$$

Given the hypothesis of small strains, a Taylor's expansion of ε_ℓ is made with respect to ε_q and only the linear terms are kept, leading to

$$\varepsilon_\ell = \sqrt{2\varepsilon_q + 1} - 1 \cong \varepsilon_q \Rightarrow \varepsilon^* = \varepsilon_\ell + C_\eta z_R - C_\zeta z_R \cong \varepsilon_q + C_\eta z_R - C_\zeta z_R, \quad (24)$$

where Eq. (17) is used and ε_q is given by Eq. (4).

Substituting Eqs. (20) and (24) into Eq. (23) and using the fact that, since the centreline contains the centroid of the cross section, the integrals $\int_A y_R \, dA$, $\int_A z_R \, dA$, $\int_A y_R^2 + z_R^2 \, dA$ and $\int_A z_R(y_R^2 + z_R^2) \, dA$ vanish, by definition, Eq. (23) is reduced to, after some algebraic manipulations,

$$\begin{aligned} \delta V_s &= \int_0^L \iint_A \delta v_s \, dA \, ds = \int_0^L \left\{ EA\varepsilon_q \delta\varepsilon_q + EI_p \left(\varepsilon_q C_\xi \delta C_\xi + \frac{C_\xi^2 \delta\varepsilon_q}{2} \right) + \right. \\ &\quad \left. + EIC_\eta \delta C_\eta + EIC_\zeta \delta C_\zeta + \frac{EI_4 C_\xi^3 \delta C_\xi}{2} + GI_p C_\xi \delta C_\xi \right\} \, ds, \end{aligned} \quad (25)$$

where $I_y = \iint_A z_R^2 \, dA$, $I_z = \iint_A y_R^2 \, dA$, $I_p = \iint_A (y_R^2 + z_R^2) \, dA$ and $I_4 = \iint_A (y_R^2 + z_R^2)^2 \, dA$.

Before their substitution in Eq. (25), the generalized curvature expressions (see Eqs. (14)) have to be written in terms of the displacements u , v , w and θ_x . This step requires a careful analysis of the orders of magnitude of all terms which appear in Eqs. (14) such that every term up to $\mathcal{O}(\varepsilon^3)$ appropriately appears in the final EOM.

Firstly, the geometrically exact expressions for θ'_y and θ'_z are written using the trivial relation $\theta' = (\sin \theta)' / \cos \theta$. Along with relations (8), one gets, after many algebraic manipulations,

$$\begin{aligned}\theta'_y &= -\frac{w''}{(1+u')} + \frac{u''w' + u'u''w' + w'^2w''}{1+3u'+3u'^2+w'^2+u'^3+u'w''^2}, \text{ and} \\ \theta'_z &= \frac{v''}{\sqrt{1+2u'+u'^2+w'^2}} - \frac{v'(u''+u'u''+v'v''+w'w'')}{(1+2u'+u'^2+v'^2+w'^2)\sqrt{1+2u'+u'^2+w'^2}}.\end{aligned}\quad (26)$$

Substituting Eqs. (26) and (8) into Eqs. (14) while using Taylor expansions to gather terms up to $\mathcal{O}(\varepsilon^3)$ leads to the final generalized curvature expressions

$$\begin{aligned}C_\xi &= \theta'_x - v'w'' + \mathcal{O}(\varepsilon^4), \\ C_\eta &= -w'' + v''\theta_x + u''w' + w'^2w'' + \frac{w''v'^2}{2} + \frac{w''\theta_x^2}{2} + u'w'' + \mathcal{O}(\varepsilon^4), \text{ and} \\ C_\zeta &= v'' + w''\theta_x - u'v'' - \frac{v''w'^2}{2} - u''v' - v'^2v'' - v'w'w'' - \frac{v''\theta_x^2}{2} + \mathcal{O}(\varepsilon^4).\end{aligned}\quad (27)$$

An important observation is that, due to the nonlinearities of C_ξ , θ_x does not provide the direct torsional angles θ along the length of the pipe. Instead, it is used to compose it along with the transverse displacements v and w , i.e., considering terms up to $\mathcal{O}(\varepsilon^3)$,

$$\theta(s) = \int_0^s C_\xi ds = \int_0^s (\theta'_x - v'w'') ds. \quad (28)$$

From here onwards, the notation $()_L = ()(s = L)$ is used. Finally, substituting Eqs. (27) into Eq. (25) leads to, after an integration with respect to the fixed time instants t_1 and t_2 , and performing multiple integrals

by parts, the final expressions for the contributions of the strain energy to the EOM:

$$\begin{aligned}
\int_{t_1}^{t_2} \delta V_s dt &= - \int_{t_1}^{t_2} \int_0^L [\delta u(V_s^{\delta u}) + \delta v(V_s^{\delta v}) + \delta w(V_s^{\delta w}) + \delta \theta_x(V_s^{\delta \theta_x})] ds dt + \\
&\quad + \int_{t_1}^{t_2} [\delta u_L(V_s^{\delta u_L}) + \delta v_L(V_s^{\delta v_L}) + \delta w_L(V_s^{\delta w_L}) + \\
&\quad + \delta \theta_{x,L}(V_s^{\delta \theta_{x,L}}) + \delta v'_L(V_s^{\delta v'_L}) + \delta w'_L(V_s^{\delta w'_L})] dt,
\end{aligned} \tag{29}$$

where

$$\begin{aligned}
V_s^{\delta u} &= \left[EA \left(u' + \frac{v'^2 + w'^2}{2} \right) + \frac{EI_p}{2} \left(\theta_x'^2 - 2\theta_x' v' w'' \right) + \right. \\
&\quad \left. + EI_y (-w'' + v'' \theta_x) w'' - EI_z (v'' + w'' \theta_x) v'' \right]' - \\
&\quad - [EI_y (-w'' + v'' \theta_x) w' - EI_z (v'' + w'' \theta_x) v']'' ,
\end{aligned} \tag{30}$$

$$\begin{aligned}
V_s^{\delta v} &= \left[EA \left(u' + \frac{v'^2 + w'^2}{2} \right) v' + \frac{EI_p}{2} \theta_x'^2 v' - EI_y v' w''^2 + \right. \\
&\quad \left. + EI_z v'' (-u'' - 2v' v'' - w' w'') - GI_p (\theta_x' - v' w'') w'' \right]' - \\
&\quad - [EI_y (-w'' + v'' \theta_x) \theta_x + EI_z (v'' + w'' \theta_x - 2u' v'' - v'' w'^2 - \\
&\quad \left. - u'' v' - 2v'^2 v'' - v' w' w'' - v'' \theta_x^2) \theta_x]'' ,
\end{aligned} \tag{31}$$

$$\begin{aligned}
V_s^{\delta w} &= \left[EA \left(u' + \frac{v'^2 + w'^2}{2} \right) w' + \frac{EI_p}{2} w' \theta_x'^2 - EI_y w'' (u'' + 2w' w'') + \right. \\
&\quad \left. + EI_z v'' (-w' v'' - v' w'') \right]' - [EI_y (w'' - v'' \theta_x - u'' w' - 2w'^2 w'' - \\
&\quad - w'' v'^2 - w'' \theta_x^2 - 2u' w'') + EI_z (v'' \theta_x - v'' v' w' + w'' \theta_x^2) - \\
&\quad \left. - GI_p (\theta_x' - v' w'') v']'' ,
\right.
\end{aligned} \tag{32}$$

$$V_s^{\delta\theta_x} = \left[EI_p \left(u' + \frac{v'^2 + w'^2}{2} \right) \theta'_x + \frac{EI_4}{2} \theta'^3 + GI_p (\theta'_x - v' w'') \right]' - \\ - \left[EI_y (-v'' w'' + \theta_x v''^2 - \theta_x w''^2) + EI_z (v'' w'' + w''^2 \theta_x - \theta_x v''^2) \right], \quad (33)$$

$$V_s^{\delta u_L} = \left[EA \left(u'_L + \frac{v'^2 + w'^2}{2} \right) + \frac{EI_p}{2} (\theta'^2_{x,L} - 2\theta'_{x,L} v'_L w''_L) + \right. \\ \left. + EI_y (-w''_L + v''_L \theta_{x,L}) w''_L - EI_z (v''_L + w''_L \theta_{x,L}) v''_L \right] - \\ - \left[EI_y (-w''_L + v''_L \theta_{x,L}) w'_L - EI_z (v''_L + w''_L \theta_{x,L}) v'_L \right]', \quad (34)$$

$$V_s^{\delta v_L} = \left[EA \left(u'_L + \frac{v'^2 + w'^2}{2} \right) v'_L + \frac{EI_p}{2} \theta'^2_{x,L} v'_L - EI_y v'_L w''^2 + \right. \\ \left. + EI_z v''_L (-u''_L - 2v'_L v''_L - w'_L w''_L) - GI_p (\theta'_{x,L} - v'_L w''_L) w''_L \right] - \\ - \left[EI_y (-w''_L + v''_L \theta_{x,L}) \theta_{x,L} + EI_z (v''_L + w''_L \theta_{x,L} - 2u'_L v''_L - v''_L w'^2 - \right. \\ \left. - u''_L v'_L - 2v'^2_L v''_L - v'_L w'_L w''_L - v''_L \theta'^2_{x,L}) \right]', \quad (35)$$

$$V_s^{\delta w_L} = \left[EA \left(u'_L + \frac{v'^2 + w'^2}{2} \right) w'_L + \frac{EI_p}{2} w'_L \theta'^2_{x,L} - EI_y w''_L (u''_L + 2w'_L w''_L) + \right. \\ \left. + EI_z v''_L (-w'_L v''_L - v'_L w''_L) \right] - \left[EI_y (w''_L - v''_L \theta_{x,L} - u''_L w'_L - 2w'^2_L w''_L - \right. \\ \left. - w''_L v'^2 - w''_L \theta'^2_{x,L} - 2u'_L w''_L) + EI_z (v''_L \theta_{x,L} - v''_L v'_L w'_L + w''_L \theta'^2_{x,L}) - \right. \\ \left. - GI_p (\theta'_{x,L} - v'_L w''_L) v'_L \right]', \quad (36)$$

$$V_s^{\delta\theta_{x,L}} = EI_p \left(u'_L + \frac{v'^2 + w'^2}{2} \right) \theta'_{x,L} + \frac{EI_4}{2} \theta'^3_{x,L} + GI_p (\theta'_{x,L} - v'_L w''_L), \quad (37)$$

$$V_s^{\delta v'_L} = \left[EI_y (-w''_L + v''_L \theta_{x,L}) \theta_{x,L} + EI_z (v''_L + w''_L \theta_{x,L} - 2u'_L v''_L - v''_L w'^2_L - u''_L v'_L - 2v'^2_L v''_L - v'_L w'_L w''_L - v''_L \theta_{x,L}^2) \right], \quad (38)$$

and

$$V_s^{\delta w'_L} = \left[EI_y (w''_L - v''_L \theta_{x,L} - u''_L w'_L - 2w'^2_L w''_L - w''_L v'^2_L - w''_L \theta_{x,L}^2 - 2u'_L w''_L) + EI_z (v''_L \theta_{x,L} - v''_L v'_L w'_L + w''_L \theta_{x,L}^2) - GI_p (\theta'_{x,L} - v'_L w''_L) v'_L \right]. \quad (39)$$

In order to obtain Eqs. (29)-(39) from Eqs. (4), (25) and (27), it is noted that, since the pipe is clamped at the inlet, $\delta u_0 = \delta v_0 = \delta w_0 = \delta v'_0 = \delta w'_0 = \delta \theta_{x,0} = 0$. Consequently, no natural boundary conditions involving these virtual displacements, at that point, are obtained.

The contribution of the gravitational potential energy to the generalized Hamilton's principle, in turn, is given by

$$\int_{t_1}^{t_2} \delta V_g dt = \int_{t_1}^{t_2} \delta \left(\int_0^L (m+M)g(-s-u) ds \right) dt = \int_{t_1}^{t_2} \int_0^L -[(m+M)g\delta u] ds dt. \quad (40)$$

The kinetic energy of the pipe T_p is now addressed and can be evaluated as

$$T_p = \iiint_V \frac{1}{2} \rho \frac{d\mathbf{r}_R}{dt} \cdot \frac{d\mathbf{r}_R}{dt} dV. \quad (41)$$

Firstly, deriving the position vector of a generic point belonging to the pipe (see Eqs. (12)) with respect to time, and recalling that (ξ, η, ζ) is a rotating reference frame, provides

$$\frac{d\mathbf{r}_R}{dt} = \dot{u}\hat{\mathbf{i}} + \dot{v}\hat{\mathbf{j}} + \dot{w}\hat{\mathbf{k}} + \boldsymbol{\omega} \times (y_R\hat{\boldsymbol{\eta}} + z_R\hat{\boldsymbol{\zeta}}), \quad (42)$$

where $\boldsymbol{\omega} = \dot{\theta}_x \hat{\boldsymbol{\xi}} + \dot{\theta}_y \hat{\boldsymbol{\eta}}_1 + \dot{\theta}_z \hat{\boldsymbol{\zeta}}_2$ is the angular velocity vector. When written in the (ξ, η, ζ) local reference frame, the expression for $\boldsymbol{\omega}$ becomes

$$\boldsymbol{\omega} = \omega_\xi \hat{\boldsymbol{\xi}} + \omega_\eta \hat{\boldsymbol{\eta}} + \omega_\zeta \hat{\boldsymbol{\zeta}}, \text{ where } \begin{cases} \omega_\xi = \dot{\theta}_x + \dot{\theta}_y \sin \theta_z \\ \omega_\eta = \dot{\theta}_y \cos \theta_z \cos \theta_x + \dot{\theta}_z \sin \theta_x \\ \omega_\zeta = -\dot{\theta}_y \cos \theta_z \sin \theta_x + \dot{\theta}_z \cos \theta_x \end{cases}. \quad (43)$$

Substituting the transformations (1) and Eq. (43) into Eq. (42) leads to

$$\begin{aligned} \frac{d\mathbf{r}_R}{dt} &= \hat{\boldsymbol{\xi}}[\dot{u} i_\xi + \dot{v} j_\xi + \dot{w} k_\xi + \omega_\eta z_R - \omega_\zeta y_R] + \\ &\quad + \hat{\boldsymbol{\eta}}[\dot{u} i_\eta + \dot{v} j_\eta + \dot{w} k_\eta - \omega_\xi z_R] + \\ &\quad + \hat{\boldsymbol{\zeta}}[\dot{u} i_\zeta + \dot{v} j_\zeta + \dot{w} k_\zeta + \omega_\xi y_R]. \end{aligned} \quad (44)$$

Using Eq. (44) and again using the facts that $\|\hat{\mathbf{i}}\|^2 = \|\hat{\mathbf{j}}\|^2 = \|\hat{\mathbf{k}}\|^2 = 1$ and that $\hat{\mathbf{i}}$, $\hat{\mathbf{j}}$ and $\hat{\mathbf{k}}$ are orthogonal to each other, Eq. (41) provides, after many algebraic manipulations,

$$\begin{aligned} T_p &= \int_0^L \frac{1}{2} [m(\dot{u}^2 + \dot{v}^2 + \dot{w}^2) + \omega_\eta^2 J_y + \omega_\zeta^2 J_z + \omega_\xi^2 J_p] ds \approx \\ &\approx \int_0^L \frac{1}{2} [m(\dot{u}^2 + \dot{v}^2 + \dot{w}^2) + \omega_\xi^2 J_p] ds \end{aligned} \quad (45)$$

where $J_z = \iint_A \rho y_R^2 dA$, $J_y = \iint_A \rho z_R^2 dA$ and $J_p = \iint_A \rho(y_R^2 + z_R^2) dA$ and, as already discussed, the rotary inertia of the cross sections are considered to be negligible.

As is previously done for the generalized curvatures in the potential strain energy, care must be taken with the orders of magnitude when evaluating ω_ξ as a function of the displacements u , v , w , and θ_x . Similarly as when considering $\dot{\theta}_y'$ and $\dot{\theta}_z'$, firstly, $\dot{\theta}_y$ is written in a geometrically exact manner using the trivial relation $\dot{\theta}_y = (\sin \theta_y)/\cos \theta_y$. Along with relations (8), after many algebraic manipulations, this leads to

$$\dot{\theta}_y = -\frac{w'}{(1+u')} + \frac{w' [w'\dot{w}' + (1+u')\dot{u}']}{1+3u'+3u'^2+w'^2+u'^3+u'w''^2}. \quad (46)$$

Substituting Eqs. (46) and (8) into Eqs. (43) while using Taylor's expansions to gather terms up to $\mathcal{O}(\varepsilon^3)$ leads to the final angular velocity expression around the ξ -axis

$$\omega_\xi = \dot{\theta}_x - v'\dot{w}' + \mathcal{O}(\varepsilon^4), \quad (47)$$

which is then substituted into Eq. (45). Evaluating the variation of the resultant expression and integrating from the fixed time instants t_1 and t_2 leads to, after performing multiple integrals by parts in both time and space domains,

$$\begin{aligned} \int_{t_1}^{t_2} \delta T_p dt &= \int_{t_1}^{t_2} \int_0^L \left\{ \delta u (-m\ddot{u}) + \delta v \left[-m\ddot{v} - J_p (v'\dot{w}'^2 - \dot{\theta}_x \dot{w}') \right] + \right. \\ &\quad + \delta w \left[-m\ddot{w} + J_p (\ddot{w}' v'^2 + 2\dot{w}' v' \dot{v}' - \ddot{\theta}_x v' - \dot{\theta}_x \dot{v}') \right] + \\ &\quad \left. + \delta \theta_x \left[-J_p (\ddot{\theta}_x - \dot{v}' \dot{w}' - v' \ddot{w}') \right] \right\} ds dt + \\ &\quad + \int_{t_1}^{t_2} \left\{ -J_p (\ddot{w}'_L v'^2_L + 2\dot{w}'_L v'_L \dot{v}'_L - \ddot{\theta}_{x,L} v'_L - \dot{\theta}_{x,L} \dot{v}'_L) \delta w_L + \right. \\ &\quad \left. + J_p (v'_L \dot{w}'^2_L - \dot{\theta}_{x,L} \dot{w}'_L) \delta v_L \right\} dt. \end{aligned} \quad (48)$$

For the integrals by parts carried out above, recall that u , v , w and θ_x are prescribed at t_1 and t_2 , and that the inlet is clamped.

Focus is now placed on the kinetic energy of the fluid T_F , which can be evaluated as

$$T_F = \iiint_V \frac{1}{2} \rho_F \mathbf{v}_F \cdot \mathbf{v}_F dV, \quad (49)$$

where \mathbf{v}_F is the velocity vector of the fluid particles, which is considered to be that of the centreline of the pipe with an additional tangential contribution due to the presence of internal flow. Thus, using the transformations (1),

$$\begin{aligned}\mathbf{v}_F = \frac{d\mathbf{r}}{dt} + U\hat{\boldsymbol{\tau}} = & [\dot{u} i_\xi + \dot{v} j_\xi + \dot{w} k_\xi + U] \hat{\boldsymbol{\xi}} + \\ & + [\dot{u} i_\eta + \dot{v} j_\eta + \dot{w} k_\eta] \hat{\boldsymbol{\eta}} + [\dot{u} i_\zeta + \dot{v} j_\zeta + \dot{w} k_\zeta] \hat{\boldsymbol{\zeta}}.\end{aligned}\quad (50)$$

Again using the facts that $\|\hat{\mathbf{i}}\|^2 = \|\hat{\mathbf{j}}\|^2 = \|\hat{\mathbf{k}}\|^2 = 1$ and that $\hat{\mathbf{i}}$, $\hat{\mathbf{j}}$ and $\hat{\mathbf{k}}$ are orthogonal to each other, the scalar product $\mathbf{v}_F \cdot \mathbf{v}_F$ can be written as, after some algebraic manipulations,

$$\mathbf{v}_F \cdot \mathbf{v}_F = U^2 + \dot{u}^2 + \dot{v}^2 + \dot{w}^2 + 2U(\dot{u} i_\xi + \dot{v} j_\xi + \dot{w} k_\xi). \quad (51)$$

The necessary transformations in Eqs. (9) are approximated using a Taylor's expansion in order to retain terms up to $\mathcal{O}(\varepsilon^3)$ and become

$$\begin{aligned}i_\xi &= 1 - \frac{v'^2}{2} - \frac{w'^2}{2} + \mathcal{O}(\varepsilon^4), \\ j_\xi &= v' - u'v' - \frac{v'^3}{2} - \frac{v'w'^2}{2} + \mathcal{O}(\varepsilon^4), \text{ and} \\ k_\xi &= w' - u'w' - \frac{v'^2w'}{2} - \frac{w'^3}{2} + \mathcal{O}(\varepsilon^4).\end{aligned}\quad (52)$$

Equations (52) are substituted into Eq. (51), and the resultant expression is then substituted into Eq. (49). The result of evaluating its variation with subsequent integration between the fixed time instants t_1 and t_2 leads to, after multiple integrals by parts in both time and space domains,

$$\begin{aligned}
\int_{t_1}^{t_2} \delta T_F dt &= \int_{t_1}^{t_2} M \left\{ [U (-v'_L \dot{v}_L - w'_L \dot{w}_L)] \delta u_L + \right. \\
&\quad + \left[U \left(-\dot{u}_L v'_L + \dot{v}_L - u'_L \dot{v}_L - \frac{3v'^2 \dot{v}_L}{2} - \frac{\dot{v}_L w'^2}{2} - \dot{w}_L w'_L v'_L \right) \right] \delta v_L + \\
&\quad + \left. \left[U \left(-\dot{u}_L w'_L - \dot{v}_L v'_L w'_L + \dot{w}_L - u'_L \dot{w}_L - \frac{v'^2 \dot{w}_L}{2} - \frac{3w'^2 \dot{w}_L}{2} \right) \right] \delta w_L \right\} dt - \\
&\quad - \int_{t_1}^{t_2} \int_0^L M \left\{ \delta u \left\{ [\ddot{u} + U (-v' \dot{v}' - w' \dot{w}')] + U (v' \dot{v} - w' \dot{w})' \right\} + \right. \\
&\quad \delta v \left\{ \left[\ddot{v} + U \left(\dot{v}' - \dot{u}' v' - u' \dot{v}' - \frac{3v'^2 \dot{v}'}{2} - \frac{\dot{v}' w'^2}{2} - v' w' \dot{w}' \right) \right] + \right. \\
&\quad + U \left(-\dot{u} v' + \dot{v} - u' \dot{v} - \frac{3v'^2 \dot{v}}{2} - \frac{\dot{v} w'^2}{2} - \dot{w} w' v' \right)' \Big\} + \\
&\quad + \delta w \left\{ \left[\ddot{w} + U \left(\dot{w}' - \dot{u}' w' - u' \dot{w}' - v' \dot{v}' w' - \frac{v'^2 \dot{w}'}{2} - \frac{3w'^2 \dot{w}'}{2} \right) \right] + \right. \\
&\quad \left. \left. + U \left(-\dot{u} w' - \dot{v} v' w' + \dot{w} - u' \dot{w} - \frac{v'^2 \dot{w}}{2} - \frac{3w'^2 \dot{w}}{2} \right)' \right\} \right\} ds dt. \tag{53}
\end{aligned}$$

Once more, the facts that u , v , w and θ_x are prescribed at t_1 and t_2 , and that the inlet is fixed, were used in the integrals by parts carried out above. Note that the classical linear fluid coriolis forces $2MU\dot{v}'$ and $2MU\dot{w}'$, in the y - and z -directions, respectively, can also be seen in Eq. (53).

Now, consider the development of the second term in Eq. (21), the virtual work done by the generalized non-conservative forces. It can be written as a sum of two different contributions, namely $\delta W = \delta W_p + \delta W_T$, where δW_p and δW_T are the virtual works done by pressure forces and by the applied torsional moment, respectively.

Given that the inlet is clamped, the cross sections are considered to move as rigid bodies and that the fluid is discharged to the atmosphere, the contribution δW_p vanishes. The reader interested in more details regarding this term is referred to Sec. 3.3 of [22].

The contribution δW_T , in turn, can be trivially written as

$$\delta W_T = \int_0^L M_T \delta(x - \bar{x}_T) \delta \theta_x ds. \quad (54)$$

Subsequently integrating Eq. (54) with respect to the fixed time instants t_1 and t_2 for its substitution in the generalized Hamilton's principle is straightforward.

Now, the development of the third term in Eq. (21), which represents the flow of momentum across the surfaces of the open volume, is made. Since $\delta \mathbf{r} = \mathbf{0}$ at S_i and, at the pipe walls (S_c), $(\mathbf{v}_F - d\mathbf{r}/dt) \cdot \mathbf{n} = U \hat{\tau} \cdot \mathbf{n} = 0$, this term is reduced to

$$\begin{aligned} & - \iint_{\partial V_o} \rho_F (\mathbf{v}_F \cdot \delta \mathbf{r}) \left(\mathbf{v}_F - \frac{d\mathbf{r}}{dt} \right) \cdot \mathbf{n} d\partial V_o = \\ & = - \rho_F A_F (\mathbf{v}_{F,L} \cdot \delta \mathbf{r}_L) \left(\mathbf{v}_{F,L} - \frac{d\mathbf{r}_L}{dt} \right) \cdot \mathbf{n}_L = \\ & = - MU (\mathbf{v}_{F,L} \cdot \delta \mathbf{r}_L). \end{aligned} \quad (55)$$

Again recalling that $\|\hat{\mathbf{i}}\|^2 = \|\hat{\mathbf{j}}\|^2 = \|\hat{\mathbf{k}}\|^2 = 1$ and that $\hat{\mathbf{i}}$, $\hat{\mathbf{j}}$ and $\hat{\mathbf{k}}$ are orthogonal to each other, Eq. (55) can be written as, using Eqs. (52),

$$\begin{aligned} & - MU (\mathbf{v}_{F,L} \cdot \delta \mathbf{r}_L) = \\ & = \delta u_L \left[-MU \dot{u}_L - MU^2 \left(1 - \frac{{v'_L}^2}{2} - \frac{{w'_L}^2}{2} \right) \right] + \\ & + \delta v_L \left[-MU \dot{v}_L - MU^2 \left({v'_L}^2 - u'_L v'_L - \frac{{v'_L}^3}{2} - \frac{{v'_L} {w'_L}^2}{2} \right) \right] + \\ & + \delta w_L \left[-MU \dot{w}_L - MU^2 \left({w'_L}^2 - u'_L w'_L - \frac{{v'_L}^2 {w'_L}}{2} - \frac{{w'_L}^3}{2} \right) \right]. \end{aligned} \quad (56)$$

A noteworthy observation is that, in mathematical models for inextensible pipes, the terms representing the fluid centrifugal forces $MU^2 v''$ and $MU^2 w''$,

in the y - and z -directions, respectively, appear explicitly in the EOM (see [8]). In extensible models, in turn, they appear in the natural boundary conditions, as shown in Eq. (56).

Considering the evaluation of the term related to the flow of kinetic energy across the open volume (fourth term in Eq. (21)), since the plug-flow model is used in the present work, the internal flow velocity is independent of the generalized velocities. As a consequence, this term is zero and thus plays no role in the resultant EOM. The reader interested in a more detailed explanation is referred to Sec. 7 of [6].

Finally, substituting Eqs. (29)-(39), (40), (48), (53), (??), (54) and (56) into the generalized Hamilton's principle (Eq. (21)) leads to a set of coupled nonlinear partial differential equations which represent the EOM and associated natural boundary conditions of the pipe conveying fluid. Before being explicitly shown, these equations are made dimensionless.

To that end, all translational displacements are normalized with respect to the length of the pipe and time is normalized as shown in Eq. (57):

$$\tau = \left(\frac{EI}{m+M} \right)^{1/2} \frac{t}{L^2}; \quad \xi = \frac{u}{L}; \quad \eta = \frac{v}{L}; \quad \zeta = \frac{w}{L}. \quad (57)$$

where, since the pipe has a circular cross section, $I_y = I_z = I$, which is used from here on. In addition, the following dimensionless quantities are defined:

$$\begin{aligned} \beta &= \frac{M}{m+M}; \quad u = \left(\frac{M}{EI} \right)^{1/2} UL; \quad \gamma = \frac{(m+M)gL^3}{EI}; \\ \kappa_0 &= \frac{M_T L}{GI_p}; \quad \kappa_1 = \frac{EI_p}{EI}; \quad \kappa_2 = \frac{EAL^2}{EI}; \quad \kappa_3 = \frac{GI_p}{EI}; \quad \kappa_4 = \frac{EI_4}{EIL^2}; \\ \kappa_5 &= \frac{J_p}{(m+M)L^2}; \quad \hat{\delta}(\xi - \bar{\xi}_T) = L\delta(x - \bar{x}_T). \end{aligned} \quad (58)$$

Using the notation $(\cdot)' = \partial(\cdot)/\partial\hat{s}$, where $\hat{s} = s/L$, and $(\cdot) = \partial(\cdot)/\partial\tau$, the dimensionless EOM and associated natural boundary conditions are obtained as:

$$\begin{aligned}
& \ddot{\xi} + \gamma - \kappa_2 \left[\xi'' + \frac{1}{2} (\eta'^2 + \zeta'^2)' \right] - \sqrt{\beta} u \left[\eta' \dot{\eta}' + \zeta' \dot{\zeta}' + (\eta' \dot{\eta} + \zeta' \dot{\zeta})' \right] - \\
& - \kappa_1 [\theta'_x \theta''_x + (\theta'_x \eta' \zeta'')]' + 2(\zeta'' \zeta''' + \eta'' \eta''') - \\
& - (\zeta'' \zeta' + \eta'' \eta' - \theta_x \eta'' \zeta' + \theta_x \zeta'' \eta')'' = 0,
\end{aligned} \tag{59}$$

governing the axial displacements ξ ,

$$\begin{aligned}
& \ddot{\eta} + \eta''''' + \sqrt{\beta} u \left[2\dot{\eta}' - \dot{\xi}' \eta' - \xi' \dot{\eta}' + \frac{3\eta'^2 \dot{\eta}'}{2} - \frac{\dot{\eta}' \zeta'^2}{2} - \eta' \zeta' \dot{\zeta}' - \right. \\
& \left. - \left(\dot{\xi} \eta' + \xi' \dot{\eta} + \frac{3\eta'^2 \dot{\eta}}{2} + \frac{\dot{\eta} \zeta'^2}{2} + \dot{\zeta} \zeta' \eta' \right)' \right] - \kappa_5 (\dot{\theta}_x \dot{\zeta}' + \eta' \dot{\zeta}'^2)' - \\
& - \kappa_2 \left[\xi' \eta' + \frac{1}{2} (\eta'^2 + \zeta'^2) \eta' \right]' + \kappa_3 (\theta'_x \zeta'' + \zeta''^2 \eta')' + \\
& + \left(\xi'' \eta'' - \frac{\kappa_1 \theta'^2 \eta'}{2} + \eta' \zeta''^2 + 2\eta''^2 \eta' + \eta'' \zeta' \zeta'' \right)' - \\
& - \left(2\xi' \eta'' + \xi'' \eta' + \eta'' \zeta'^2 + 2\eta'^2 \eta'' + \eta' \zeta' \zeta'' \right)'' = 0,
\end{aligned} \tag{60}$$

governing the transverse displacements η ,

$$\begin{aligned}
& \ddot{\zeta} + \zeta''''' + \sqrt{\beta} u \left[2\dot{\zeta}' - \dot{\xi}' \zeta' - \xi' \dot{\zeta}' - \eta' \dot{\eta}' \zeta' - \frac{\eta'^2 \dot{\zeta}'}{2} - \right. \\
& \left. - \frac{3\zeta'^2 \dot{\zeta}'}{2} - \left(\dot{\xi} \zeta' + \xi' \dot{\zeta} + \dot{\eta} \eta' \zeta' + \frac{\eta'^2 \dot{\zeta}}{2} + \frac{3\zeta'^2 \dot{\zeta}}{2} \right)' \right] + \kappa_5 (\ddot{\theta}_x \eta' + \dot{\theta}_x \dot{\eta}' - \\
& - \ddot{\zeta} \eta'^2 - 2\dot{\zeta}' \eta' \dot{\eta}')' - \kappa_2 \left[\xi' \zeta' + \frac{1}{2} (\eta'^2 + \zeta'^2) \zeta' \right]' - \kappa_3 (\theta'_x \eta' + \eta'^2 \zeta'')'' + \\
& + \left(\xi'' \zeta'' - \frac{\kappa_1 \theta'^2 \zeta'}{2} + 2\zeta' \zeta''^2 + \zeta' \eta''^2 + \eta' \eta'' \zeta'' \right)' - \\
& - \left(\xi'' \zeta' + 2\xi' \zeta'' + 2\zeta'^2 \zeta'' + \zeta'' \eta'^2 + \eta'' \eta' \zeta' \right)'' = 0,
\end{aligned} \tag{61}$$

governing the transverse displacements ζ ,

$$\begin{aligned} \kappa_5 \ddot{\theta}_x - \kappa_0 \kappa_3 \hat{\delta}(\xi - \bar{\xi}_T) - \kappa_3 [\theta''_x - (\eta' \zeta'')'] - \kappa_5 (\dot{\eta}' \dot{\zeta}' + \eta' \ddot{\zeta}') - \\ - \kappa_1 \left[\xi' \theta'_x + \frac{1}{2} (\eta'^2 + \zeta'^2) \theta'_x \right]' - \frac{\kappa_4 (\theta'^3_x)' }{2} = 0, \end{aligned} \quad (62)$$

governing the torsional displacements θ_x . Using the notation $(\cdot)_{0,1} = (\cdot)(\hat{s} = 0, 1)$, the generalized Hamilton's principle also provides the following natural boundary conditions:

$$\begin{aligned} \kappa_2 \xi'_1 + \sqrt{\beta} u \left(\dot{\xi}_1 + \eta'_1 \dot{\eta}_1 + \zeta'_1 \dot{\zeta}_1 \right) + \frac{\kappa_2}{2} \left(\eta'_1 + \zeta'^2_1 \right) + \kappa_1 \left(\frac{\theta'^2_{x,1}}{2} - \theta'_{x,1} \zeta''_1 \eta'_1 \right) - \\ - \zeta''^2_1 - \eta''^2_1 + (\zeta''_1 \zeta'_1 + \eta''_1 \eta'_1 - \theta'_{x,1} \eta''_1 \zeta'_1 + \theta_{x,1} \zeta''_1 \eta'_1)' - \\ - \frac{u^2}{2} \left(\eta'_1 + \zeta'^2_1 \right) + u^2 = 0, \end{aligned} \quad (63)$$

at ξ_1 ,

$$\begin{aligned} \kappa_2 \left[\xi'_1 \eta'_1 + \frac{1}{2} (\eta'_1 + \zeta'^2_1) \eta'_1 \right] - \eta'''_1 + \sqrt{\beta} u \left(\dot{\xi}_1 \eta'_1 + \xi'_1 \dot{\eta}_1 + \frac{3 \eta'^2_1 \dot{\eta}_1}{2} + \frac{\dot{\eta}_1 \zeta'^2_1}{2} + \right. \\ \left. + \dot{\zeta}_1 \zeta'_1 \eta'_1 \right) + \kappa_5 \left(\dot{\theta}_{x,1} \dot{\zeta}'_1 - \eta'_1 \dot{\zeta}'^2_1 \right) + \kappa_3 \left(-\theta'_{x,1} \zeta''_1 + \eta'_1 \zeta''^2_1 \right) + \frac{\kappa_1 \theta'^2_{x,1} \eta'_1}{2} - \xi''_1 \eta''_1 - \\ - \eta'_1 \zeta''^2_1 - 2 \eta''^2_1 \eta'_1 - \zeta'_1 \zeta''_1 \eta''_1 + \left(2 \xi'_1 \eta''_1 + \xi''_1 \eta'_1 + \eta''_1 \zeta'^2_1 + 2 \eta'^2_1 \eta''_1 + \eta'_1 \zeta'_1 \zeta''_1 \right)' + \\ + u^2 \left(\eta'_1 - \xi'_1 \eta'_1 - \frac{\eta'^3_1}{2} - \frac{\eta'_1 \zeta'^2_1}{2} \right) = 0 \end{aligned} \quad (64)$$

at η_1 ,

$$\begin{aligned}
& \kappa_2 \left[\xi'_1 \zeta'_1 + \frac{1}{2} \left(\eta'_1 + \zeta'^2_1 \right) \zeta'_1 \right] - \zeta'''_1 + \sqrt{\beta} u \left(\dot{\xi}_1 \zeta'_1 + \xi'_1 \dot{\zeta}_1 + \dot{\eta}_1 \eta'_1 \zeta'_1 + \frac{\eta'^2_1 \dot{\zeta}_1}{2} + \right. \\
& \left. + \frac{3\zeta'^2_1 \dot{\zeta}_1}{2} \right) - \kappa_5 \left(\ddot{\theta}_{x,1} \eta'_1 + \dot{\theta}_{x,1} \dot{\eta}'_1 - \ddot{\zeta}_1 \eta'^2_1 - 2\dot{\zeta}'_1 \eta'_1 \dot{\eta}'_1 \right) + \kappa_3 \left(\theta'_{x,1} \eta'_1 - \eta'^2_1 \zeta''_1 \right)' + \\
& + \frac{\kappa_1 \theta'^2_{x,1} \zeta'_1}{2} - \xi''_1 \zeta''_1 - 2\zeta'_1 \zeta''^2_1 - \eta''^2_1 \zeta'_1 - \eta'_1 \eta''_1 \zeta''_1 + \left(\xi''_1 \zeta'_1 + 2\xi'_1 \zeta''_1 + 2\zeta'^2_1 \zeta''_1 + \right. \\
& \left. + \zeta''_1 \eta'^2_1 + \eta''_1 \eta'_1 \zeta'_1 \right)' + u^2 \left(\zeta'_1 - \xi'_1 \zeta'_1 - \frac{\eta'^2_1 \zeta'_1}{2} - \frac{\zeta'^3_1}{2} \right) = 0,
\end{aligned} \tag{65}$$

at ζ'_1 ,

$$\kappa_3 \left(\theta'_{x,1} - \eta'_1 \zeta''_1 \right) + \kappa_1 \left[\xi'_1 \theta'_{x,1} + \frac{1}{2} \left(\eta'_1 + \zeta'^2_1 \right) \theta'_{x,1} \right] + \frac{\kappa_4 \theta'^3_{x,1}}{2} = 0, \tag{66}$$

at $\theta_{x,1}$,

$$\eta''_1 - 2\xi'_1 \eta''_1 - \xi''_1 \eta'_1 - \eta''_1 \zeta'^2_1 - 2\eta'^2_1 \eta''_1 - \eta'_1 \zeta'_1 \zeta''_1 = 0, \tag{67}$$

at η'_1 ,

$$\zeta''_1 - 2\xi'_1 \zeta''_1 - \xi''_1 \zeta'_1 - \kappa_3 \left(\theta'_{x,1} \eta'_1 - \eta'^2_1 \zeta''_1 \right) - 2\zeta'^2_1 \zeta''_1 - \eta''_1 \eta'_1 \zeta'_1 - \zeta''_1 \eta'^2_1 = 0, \tag{68}$$

at ζ'_1 . In the EOM and natural boundary conditions shown above, the dynamics of the pipe conveying fluid is not yet formulated around the static solutions for the axial and torsional solutions. This procedure, as well as other methodological aspects related to numerical simulations, are described in the next section.

3. Methodology

This section describes the methodology with which the results shown in Sec. 4 are obtained. Firstly, in Subsec. 3.1, the methods used for obtaining the axial and torsional static solutions of the nonlinear system are

described. Then, using the evaluated static solutions as an input, in Subsec. 3.2, the complete mathematical model derived in Sec. 2 is discretized using the Galerkin's method. Also shown in Sec. 3.2 are the resultant set of four coupled nonlinear ordinary differential equations. Finally, in Sec. 3.3, a discussion is made on the mathematical asymmetries seen on the EOM and associated natural boundary conditions. This discussion includes the reasons for their existence, as well as a simulation which indicates that this asymmetry is merely a mathematical one.

3.1. Evaluation of the axial and torsional static solutions

Due to the presence of gravity and internal flow, the axial displacements ξ can be separated into static and dynamic parts. Analogously, due to the presence of a torsional moment applied at a point along the length of the pipe, the same applies to the torsional displacements θ_x . Accordingly, the dynamics is formulated around these static solutions, i.e.

$$\xi = \xi_s + \xi_d \text{ and } \theta_x = \theta_{x,s} + \theta_{x,d}. \quad (69)$$

Due to the static solutions possibly having discontinuous derivatives (as is shown further on in this subsection), the static problem cannot be formulated using a single spatial domain. With this in mind, the first step is to write the generalized Hamilton's principle for the static scenario and prior to the integrals by parts procedure, i.e.

$$\begin{aligned} & \int_{\tau_1}^{\tau_2} \left\{ \int_0^1 \left\{ \delta \xi'_s \left(-\kappa_2 \xi'_s - \frac{\kappa_1 \theta'^2_{x,s}}{2} \right) + \delta \theta'_{x,s} \left(-\kappa_1 \xi'_s \theta'_{x,s} - \frac{\kappa_4 \theta'^3_{x,s}}{2} - \kappa_3 \theta'_{x,s} \right) \right\} d\hat{s} + \right. \\ & \quad \left. + \delta \xi_{s,1} (-u^2) + \int_0^1 \delta \xi_s (\gamma) d\hat{s} + \delta \theta_{x,s,\bar{\xi}_T} (\kappa_0 \kappa_3) \right\} d\tau = 0. \end{aligned} \quad (70)$$

Both static solutions are subsequently divided into two parts, namely one before and one after the point at which the torsional moment is applied to, so that

$$\xi_s = \begin{cases} {}^{(1)}\xi_s, & \text{for } 0 \leq \hat{s} \leq \bar{\xi}_T \\ {}^{(2)}\xi_s, & \text{for } \bar{\xi}_T \leq \hat{s} \leq 1 \end{cases}, \quad \text{and } \theta_{x,s} = \begin{cases} {}^{(1)}\theta_{x,s}, & \text{for } 0 \leq \hat{s} \leq \bar{\xi}_T \\ {}^{(2)}\theta_{x,s}, & \text{for } \bar{\xi}_T \leq \hat{s} \leq 1 \end{cases}. \quad (71)$$

Additionally, since the axial and torsional displacements are continuous, ${}^{(1)}\xi_{s,\bar{\xi}_T} = {}^{(2)}\xi_{s,\bar{\xi}_T}$ and ${}^{(1)}\theta_{x,s,\bar{\xi}_T} = {}^{(2)}\theta_{x,s,\bar{\xi}_T}$. Then, after multiple integrals by parts and regrouping of the terms, Eq. (70) becomes

$$\begin{aligned} & \int_0^{\bar{\xi}} \left\{ \delta {}^{(1)}\xi_s \left(\kappa_2 {}^{(1)}\xi_s'' + \kappa_1 {}^{(1)}\theta'_{x,s} {}^{(1)}\theta''_{x,s} + \gamma \right) + \right. \\ & \quad \left. + \delta {}^{(1)}\theta_{x,s} \left[\kappa_1 \left({}^{(1)}\xi'_s {}^{(1)}\theta'_{x,s} \right)' + \frac{\kappa_4}{2} \left({}^{(1)}\theta'^3_{x,s} \right)' + \kappa_3 {}^{(1)}\theta''_{x,s} \right] \right\} d\hat{s} + \\ & \int_{\bar{\xi}}^1 \left\{ \delta {}^{(2)}\xi_s \left(\kappa_2 {}^{(2)}\xi_s'' + \kappa_1 {}^{(2)}\theta'_{x,s} {}^{(2)}\theta''_{x,s} + \gamma \right) + \right. \\ & \quad \left. + \delta {}^{(2)}\theta_{x,s} \left[\kappa_1 \left({}^{(2)}\xi'_s {}^{(2)}\theta'_{x,s} \right)' + \frac{\kappa_4}{2} \left({}^{(2)}\theta'^3_{x,s} \right)' + \kappa_3 {}^{(2)}\theta''_{x,s} \right] \right\} d\hat{s} + \\ & \delta {}^{(1),(2)}\xi_{s,\bar{\xi}} \left(-\kappa_2 {}^{(1)}\xi'_{s,\bar{\xi}} - \frac{\kappa_1 {}^{(1)}\theta'^2_{x,s,\bar{\xi}}}{2} + \kappa_2 {}^{(2)}\xi'_{s,\bar{\xi}} + \frac{\kappa_1 {}^{(2)}\theta'^2_{x,s,\bar{\xi}}}{2} \right) + \\ & + \delta {}^{(2)}\xi_{s,1} \left(-\kappa_2 {}^{(2)}\xi'_{s,1} - \frac{\kappa_1 {}^{(2)}\theta'^2_{x,s,1}}{2} - u^2 \right) + \\ & + \delta {}^{(1),(2)}\theta_{x,s,\bar{\xi}} \left(-\kappa_1 {}^{(1)}\xi'_{s,\bar{\xi}} {}^{(1)}\theta'_{x,s,\bar{\xi}} - \frac{\kappa_4 {}^{(1)}\theta'^3_{x,s,\bar{\xi}}}{2} - \kappa_3 {}^{(1)}\theta'_{x,s,\bar{\xi}} + \right. \\ & \quad \left. + \kappa_1 {}^{(1)}\xi'_{s,\bar{\xi}} {}^{(1)}\theta'_{x,s,\bar{\xi}} + \frac{\kappa_4 {}^{(1)}\theta'^3_{x,s,\bar{\xi}}}{2} + \kappa_3 {}^{(1)}\theta'_{x,s,\bar{\xi}} + \kappa_0 \kappa_3 \right) + \\ & + \delta {}^{(2)}\theta_{x,s,1} \left(\kappa_1 {}^{(2)}\xi'_{s,1} {}^{(2)}\theta'_{x,s,1} + \frac{\kappa_4 {}^{(2)}\theta'^3_{x,s,1}}{2} + \kappa_3 {}^{(2)}\theta'_{x,s,1} \right) = 0. \quad (72) \end{aligned}$$

Note that, if the left hand side of Eq. (70) is equal to zero when integrated between the fixed time instants τ_1 and τ_2 , then it must always be zero due to its inherent independence of time. Equation (72) shows that, while the axial generalized coordinates are coupled to the torsional ones by nonlinear terms, the generalized coordinates for different space domains are coupled by the natural boundary conditions at $\bar{\xi}$. More specifically, in the axial

direction, this shared natural boundary condition represents the difference in the normal force, before and after $\bar{\xi}$, due to the nonlinear coupling with torsion. In the torsional direction, on the other hand, this shared natural boundary condition indicates that the difference in torsional moments, before and after $\bar{\xi}$, is equal to the applied localized torsional moment. The resultant ordinary differential equations are discretized using Galerkin's method, i.e.

$$\begin{aligned} {}^{(1)}\xi_s(\hat{s}) &= \sum_{n=1}^{N_{as}} {}^{(1)}A_{s,n} {}^{(1)}\phi_{s,n}(\hat{s}), \quad {}^{(1)}\theta_{x,s}(\hat{s}) = \sum_{n=1}^{N_{rs}} {}^{(1)}D_{s,n} {}^{(1)}\Theta_{s,n}(\hat{s}), \\ {}^{(2)}\xi_s(\hat{s}) &= \sum_{n=1}^{N_{as}} {}^{(2)}A_{s,n} {}^{(2)}\phi_{s,n}(\hat{s}) \text{ and } {}^{(2)}\theta_{x,s}(\hat{s}) = \sum_{n=1}^{N_{rs}} {}^{(2)}D_{s,n} {}^{(2)}\Theta_{s,n}(\hat{s}). \end{aligned} \quad (73)$$

where ${}^{(1)}\phi_{s,n} = {}^{(2)}\phi_{s,n} = \hat{s}^n$, for $n = 1, \dots, N_{as}$, and ${}^{(1)}\Theta_{s,n} = {}^{(2)}\Theta_{s,n} = \hat{s}^n$, for $n = 1, \dots, N_{rs}$. Thus, while modal shapes are used in discretizing the complete dynamical EOM, as is detailed in the following subsection, polynomial functions are used when approximations for the static solutions are sought.

This procedure leads to a set of nonlinear algebraic equations on the constants ${}^{(1)}A_{s,n}$ and ${}^{(2)}A_{s,n}$, for $n = 1, \dots, N_{as}$, and ${}^{(1)}\Theta_{s,n}$ and ${}^{(2)}\Theta_{s,n}$, for $n = 1, \dots, N_{rs}$. These equations are solved numerically using the fsolve function of Matlab®. As usual, initial guesses for these constants must be given to the algorithm, and the analytical solutions of the linearized problem are provided. These are denoted by ξ_s^{an} and $\theta_{x,s}^{\text{an}}$ and can be trivially obtained as

$$\begin{aligned} \xi_s^{\text{an}} &= \begin{cases} -\frac{\gamma}{2\kappa_2}\hat{s}^2 + \frac{(\gamma - u^2)}{\kappa_2}\hat{s}, & \text{for } 0 \leq \hat{s} \leq \bar{\xi} \\ -\frac{\gamma}{2\kappa_2}\hat{s}^2 + \frac{(\gamma - u^2)}{\kappa_2}\hat{s}, & \text{for } \bar{\xi} \leq \hat{s} \leq 1 \end{cases} \quad \text{and} \\ \theta_{x,s}^{\text{an}} &= \begin{cases} \kappa_0\hat{s} + \frac{\kappa_0\kappa_3}{\hat{C}_{s,x}}, & \text{for } 0 \leq \hat{s} \leq \bar{\xi}_T \\ \frac{\kappa_0\kappa_3}{\hat{C}_{s,x}} + \kappa_0\hat{\xi}_T, & \text{for } \bar{\xi}_T \leq \hat{s} \leq 1 \end{cases}, \end{aligned} \quad (74)$$

and are used as a comparison in the results shown in this section. In Eqs. (74), notice that, since linearizing the problem leads to two uncoupled solutions, the correspondent axial static solutions are given by only one expression, for both spatial domains.

Although the analytical solutions of the linearized problem are only used as initial guesses for the `fsolve` algorithm and for visual comparison, they can provide useful physical interpretations. As is shown in Eqs. (74), for the axial static solution, gravity tends to extend the pipe while the internal flow compresses it. For the torsional static solution, in turn, before the point at which the torsional moment is applied to, the solution is that of a rod with a torsional moment application modeled using the classical Saint-Venant theory. After this attachment point, the twist angle is intuitively kept constant.

Before the end of this section, a few examples for the obtained static solutions are shown with the objective of displaying the nature of the nonlinear interactions between the axial and torsional displacements. To that end, in each one, the numerical solutions for the nonlinear coupled problem are compared to the analytical ones of the linearized problem. For these examples, the relevant parameters kept fixed are $\kappa_1 = 2$, $\kappa_3 = 0.7$, $\kappa_4 = 0.001$ and $N_{as} = N_{rs} = 4$. The parameter κ_2 is set to 10000 in order to impose a near-inextensibility behavior to the pipe. The parameters that vary between each one are γ , u , κ_0 and $\bar{\xi}_T$.

To show the nonlinear effects that the torsional displacements have in the axial ones, consider first the case in which $\gamma = 0$ (horizontal pipe), $u = 0$ (no internal flow), $\kappa_0 = 2\pi$ and $\bar{\xi}_T = 0.5$. This scenario is shown in Fig. 6.

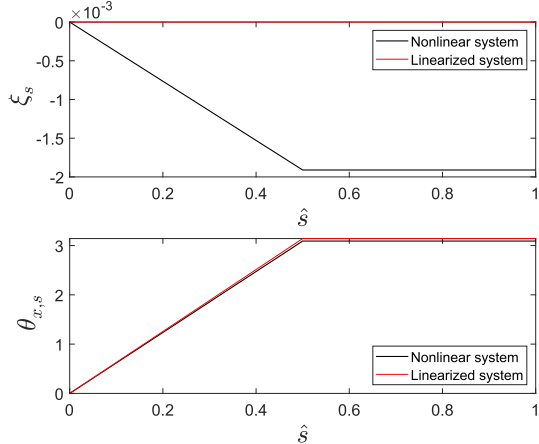


Figure 6: Comparison between the axial and torsional static solutions for the nonlinear problem (numerical solution; black) and for the linearized problem (analytical solution; red) for the case in which $\gamma = 0$, $u = 0$, $\kappa_0 = 2\pi$ and $\bar{\xi}_T = 0.5$.

Since the analytical solutions of the linearized problem do not take into account the interactions between both displacement fields, there is a large qualitative discrepancy between both axial solutions, in this case. The presence of torsional displacements induces negative axial displacements, and thus shortens the pipe. After the point at which the torsional moment is applied to, both solutions present constant values. It is worth mentioning that the torsional stiffness is slightly larger for the nonlinear problem than for the linear one (hardening nonlinearity). This difference increases with the magnitude of the torsional displacements.

Now, to solely evaluate the effects that the axial displacements have in the torsional ones, consider the case in which $\gamma = 200$ (vertical pipe), $u = 0$ (no internal flow), $\kappa_0 = 2\pi$ and $\bar{\xi}_T = 0.5$. This scenario, in turn, is shown in Fig. 7 (a). Considering the axial displacements, the difference increases from $\hat{s} = 0$ to $\hat{s} = \bar{\xi}_T$ and the pipe elongates less when the nonlinear problem is considered due to the torsion-induced negative displacements. From $\hat{s} = \bar{\xi}_T$ to $\hat{s} = 1$, as the torsional displacements are kept constant, both solutions for the axial displacements are parallel. For the torsional displacements, note that the presence of a tensile force on the pipe increases its torsional stiffness. Along with the nonlinear hardening effect, this contributes to smaller displacements along the whole length of the pipe.

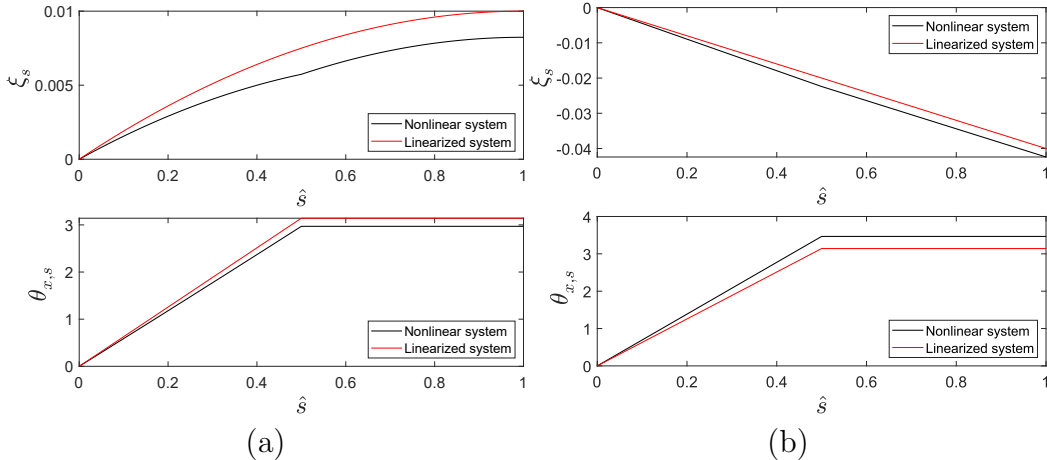


Figure 7: Comparison between the axial and torsional static solutions for the nonlinear problem (numerical solution; black) and for the linearized problem (analytical solution; red) for the cases in which (a) $\gamma = 200$, $u = 0$, $\kappa_0 = 2\pi$ and $\bar{\xi}_T = 0.5$; (b) $\gamma = 0$, $u = 20$, $\kappa_0 = 2\pi$ and $\bar{\xi} = 0.5$.

Now, a case in which the pipe is compressed is considered. The static solutions for the case in which $\gamma = 0$ (horizontal pipe), $u = 20$ (high albeit typical internal flow velocity), $\kappa_0 = 2\pi$ and $\bar{\xi}_T = 0.5$ are shown in Fig. 7 (b). Now, the strong fluid-induced compressive force is seen to noticeably decrease the torsional stiffness of the pipe. As when considering the other cases, the torsional displacements induce negative axial displacements, and thus both axial solutions are not parallel within $\hat{s} = 0$ and $\hat{s} = \bar{\xi}_T$.

Along the simulations carried out in the present work, it became clear that the quality with which the static solutions are determined plays a significant role in subsequent analyses, such as stability analyses with respect to the internal flow. More specifically, if the static solutions are not updated as u is increased, flutter never takes place. For this reason, and because the effects of the nonlinearities can be considerable, the numerical solution of the nonlinear problem is used in every result shown from here on.

The static solutions discussed in this section are an input to the subsequent dynamical analyses. Accordingly, Eqs. (71) are substituted in the EOM and associated natural boundary conditions (Eqs. (59)-(68)) and the dynamical analyses concern the dynamical displacement fields ξ_d , η , ζ and $\theta_{x,d}$.

3.2. Discretization of the dynamical equations of motion and resultant ordinary differential equations

This section presents the discretization of the complete set of dynamical EOM and associated natural boundary conditions derived in Sec. 2. Then, the resultant ordinary differential equations obtained are shown. Following the procedure of the Galerkin's method, each displacement field is approximated as a sum of products of one time-dependent function and another space-dependant:

$$\begin{aligned}\xi_d(\hat{s}, \tau) &= \sum_{n=1}^{N_a} A_n(\tau) \phi_n(\hat{s}); \quad \eta(\hat{s}, \tau) = \sum_{n=1}^{N_t} B_n(\tau) \psi_n(\hat{s}); \\ \zeta(\hat{s}, \tau) &= \sum_{n=1}^{N_t} C_n(\tau) \psi_n(\hat{s}); \quad \theta_{x,d}(\hat{s}, \tau) = \sum_{n=1}^{N_r} D_n(\tau) \Theta_n(\hat{s}).\end{aligned}\quad (75)$$

The shape functions ϕ_n , for $n = 1, \dots, (N_a - 1)$, are the axial modal shapes of a horizontal fixed-free rod. The transverse shape functions ψ_n , for

$n = 1, \dots, N_t$, in turn, are the bending modal shapes of a horizontal Euler-Bernoulli cantilevered beam. Finally, the torsional shape functions Θ_n , for $n = 1, \dots, (N_r - 1)$, are the torsional modal shapes of a fixed-free rod. The explicit expressions for each are

$$\begin{aligned}\phi_n &= \sin\left(\frac{\pi(2n-1)}{2}\hat{s}\right), \text{ for } n = 1, \dots, (N_a - 1), \\ \psi_n &= \frac{1}{2}\{\cosh(\lambda_n\hat{s}) - \cos(\lambda_n\hat{s}) - \sigma_n[\sinh(\lambda_n\hat{s}) - \sin(\lambda_n\hat{s})]\}, \text{ for } n = 1, \dots, N_t, \\ \text{and } \Theta_n &= \sin\left(\frac{\pi(2n-1)}{2}\hat{s}\right), \text{ for } n = 1, \dots, (N_r - 1).\end{aligned}\quad (76)$$

The value for the coefficients λ_n are the roots of the equation $\cos(\lambda)\cosh(\lambda) + 1 = 0$ and the values of σ_n are subsequently obtained as

$$\sigma_n = \frac{\cosh(\lambda_n) + \cos(\lambda_n)}{\sinh(\lambda_n) + \sin(\lambda_n)}. \quad (77)$$

Now, a discussion is made on an additional modification which was seen necessary along the simulations of the present model, which is the use of axial and torsional shapes to prevent excessive initial strain energy in the pipe. More specifically, the last shape function used in discretizing ξ_d is always the one corresponding to the inextensibility condition (see [12]). Additionally, as is discussed in Sec. 2.4, due to the use of nonlinear curvatures in the mathematical model, the torsional displacement field θ_x does not always correspond to the real torsional angles along the pipe. Instead, contributing to the latter angular displacements are also the transverse displacements v and w (see Eq. (28)). If the configuration of the pipe is fully contained within the (x, y) - or (x, z) -planes, then θ_x does coincide with the real torsional angles.

Consequently, while the inextensibility shape is always used for discretizing the axial dynamical displacements, the no-real-torsion shape for θ_x is used only if the initial conditions given lead to an initial configuration which does not belong to the (x, y) - or (x, z) -planes. The explicit expressions for the two shapes discussed above are

$$\begin{aligned}\phi_{N_a}(\hat{s}) &= \int_0^{\hat{s}} \left(-\frac{\eta(\hat{s}, \tau = 0)'^2}{2} - \frac{\zeta(\hat{s}, \tau = 0)'^2}{2} \right) d\hat{s}, \text{ and} \\ \Theta_{N_r}(\hat{s}) &= \int_0^{\hat{s}} \eta(\hat{s}, \tau = 0)' \zeta(\hat{s}, \tau = 0)'' d\hat{s}. \end{aligned}\quad (78)$$

By substituting the approximations given by Eqs. (75), as well as the static/dynamical displacements separation made in Eqs. (73), into the final expression for the dimensionless generalized Hamilton's principle, which can be promptly assembled from Eqs. (59)-(68), the final set of $N_a + 2N_t + N_r$ coupled nonlinear ordinary differential equations can be obtained as, using the Einstein's summation notation,

$$\begin{aligned}\ddot{A}_n \mathbf{V}_{n,m}^{(1)} + \dot{A}_n \mathbf{V}_{k,n}^{(2)} + A_n \mathbf{V}_{n,m}^{(3)} + D_n \mathbf{V}_{k,n}^{(4)} + B_n B_m \mathbf{V}_{k,n,m}^{(5)} + C_n C_m \mathbf{V}_{k,n,m}^{(6)} + \\ + D_n D_m \mathbf{V}_{k,n,m}^{(7)} + B_n C_m \mathbf{V}_{k,n,m}^{(8)} + \dot{B}_n B_m \mathbf{V}_{k,n,m}^{(9)} + \dot{C}_n C_m \mathbf{V}_{k,n,m}^{(10)} + \\ + B_n C_m D_p \mathbf{V}_{k,n,m,p}^{(11)} = 0, \end{aligned}\quad (79)$$

governing the generalized coordinates A_n ,

$$\begin{aligned}\ddot{B}_n \mathbf{V}_{k,n}^{(12)} + \dot{B}_n \mathbf{V}_{k,n}^{(13)} + B_n \mathbf{V}_{k,n}^{(14)} + C_n \mathbf{V}_{k,n}^{(15)} + A_n B_m \mathbf{V}_{k,n,m}^{(16)} + B_n D_m \mathbf{V}_{k,n,m}^{(17)} + \\ + C_n D_m \mathbf{V}_{k,n,m}^{(18)} + \dot{A}_n B_m \mathbf{V}_{k,n,m}^{(19)} + A_n \dot{B}_m \mathbf{V}_{k,n,m}^{(20)} + \dot{C}_n \dot{D}_m \mathbf{V}_{k,n,m}^{(21)} + \\ + B_n B_m B_p \mathbf{V}_{k,n,m,p}^{(22)} + B_n C_m C_p \mathbf{V}_{k,n,m,p}^{(23)} + B_n D_m D_p \mathbf{V}_{k,n,m,p}^{(24)} + \\ + \dot{B}_n B_m B_p \mathbf{V}_{k,n,m,p}^{(25)} + \dot{B}_n C_m C_p \mathbf{V}_{k,n,m,p}^{(26)} + B_n \dot{C}_m C_p \mathbf{V}_{k,n,m,p}^{(27)} + \\ + B_n \dot{C}_m \dot{C}_p \mathbf{V}_{k,n,m,p}^{(28)} = 0, \end{aligned}\quad (80)$$

governing the generalized coordinates B_n ,

$$\begin{aligned}
& \ddot{C}_n \mathbf{V}_{k,n}^{(29)} + \dot{C}_n \mathbf{V}_{k,n}^{(30)} + C_n \mathbf{V}_{k,n}^{(31)} + B_n \mathbf{V}_{k,n}^{(32)} + A_n C_m \mathbf{V}_{k,n,m}^{(33)} + C_n D_m \mathbf{V}_{k,n,m}^{(34)} + \\
& + B_n D_m \mathbf{V}_{k,n,m}^{(35)} + \dot{A}_n C_m \mathbf{V}_{k,n,m}^{(36)} + A_n \dot{C}_m \mathbf{V}_{k,n,m}^{(37)} + \dot{B}_n \dot{D}_m \mathbf{V}_{k,n,m}^{(38)} + \\
& + B_n \ddot{D}_m \mathbf{V}_{k,n,m}^{(39)} + C_n C_m C_p \mathbf{V}_{k,n,m,p}^{(40)} + B_n B_m C_p \mathbf{V}_{k,n,m,p}^{(41)} + C_n D_m D_p \mathbf{V}_{k,n,m,p}^{(42)} + \\
& + \dot{C}_n C_m C_p \mathbf{V}_{k,n,m,p}^{(43)} + B_n B_m \dot{C}_p \mathbf{V}_{k,n,m,p}^{(44)} + B_n \dot{B}_m C_p \mathbf{V}_{k,n,m,p}^{(45)} + \\
& + B_n \dot{B}_m \dot{C}_p \mathbf{V}_{k,n,m,p}^{(46)} + B_n B_m \ddot{C}_p \mathbf{V}_{k,n,m,p}^{(47)} = 0,
\end{aligned} \tag{81}$$

governing the generalized coordinates C_n , and

$$\begin{aligned}
& \ddot{D}_n \mathbf{V}_{k,n}^{(49)} + D_n \mathbf{V}_{k,n}^{(51)} + A_n \mathbf{V}_{k,n}^{(52)} + D_n D_m \mathbf{V}_{k,n,m}^{(53)} + A_n D_m \mathbf{V}_{k,n,m}^{(54)} + \\
& + B_n B_m \mathbf{V}_{k,n,m}^{(55)} + C_n C_m \mathbf{V}_{k,n,m}^{(56)} + B_n C_m \mathbf{V}_{k,n,m}^{(57)} + \dot{B}_n \dot{C}_m \mathbf{V}_{k,n,m}^{(58)} + \\
& + B_n \ddot{C}_m \mathbf{V}_{k,n,m}^{(59)} + D_n D_m D_p \mathbf{V}_{k,n,m,p}^{(60)} + B_n B_m D_p \mathbf{V}_{k,n,m,p}^{(61)} + \\
& + C_n C_m D_p \mathbf{V}_{k,n,m,p}^{(62)} = 0,
\end{aligned} \tag{82}$$

governing the generalized coordinates D_n . Due to their length, the explicit expressions for each component of the tensors $\mathbf{V}^{(1)} - \mathbf{V}^{(62)}$ are given in Appendix A. Whenever numerical integrations of Eqs. (79)-(82) are presented, they are obtained using the ode45 function in Matlab®.

3.3. Discussion on the mathematical asymmetries of the equations of motion

In this section, the reasons for the existence of the mathematical asymmetries seen in the EOM and associated natural boundary conditions, in terms of both transverse displacements η and ζ , are more clearly outlined. Additionally, it is shown that said asymmetries are merely mathematical and do not imply in an asymmetric dynamical response from the pipe conveying fluid.

Firstly, considering the developments made in Sec. 2, note that there are two sources for asymmetries in the EOM: the kinetic and potential strain energies of the pipe. There are two reasons for the existence of these asymmetries: (i) the use of Euler angles to describe the kinematics of the system and (ii) the use of nonlinear expressions for generalized curvature expressions (Eqs. (27)) and for the angular velocity around the x -axis (Eq. (47)).

To evaluate the symmetry of the dynamical response of the pipe, consider the simple free and undamped vibrations scenario characterized by the

parameters $\gamma = 0$ (horizontal pipe), $u = 0$ (no internal flow and thus the mass-ratio β is irrelevant), $\kappa_0 = 0$ (no applied torsional moment), $\kappa_1 = 2$, $\kappa_3 = 0.7$ and $\kappa_4 = 0.001$. The number of shape functions used for obtaining the static and dynamical solutions are $N_{as} = N_{rs} = 4$ and $N_a = 3$, $N_t = 8$ and $N_r = 4$, respectively.

Most importantly, the initial conditions given are $B_1 = C_1 = 0.5/\sqrt{2}$, i.e. planar initial conditions belonging to a vertical plane inclined 45° with respect to the y - and z -axes and such that a maximum amplitude of 0.5 occurs on the first transverse modal shape of the pipe. Given that all asymmetries consist of nonlinear terms, the large-amplitude initial conditions are given with the objective of increasing the effects of the nonlinearities. The resultant time series for ξ_d , η , ζ and $\theta_{x,d}$ at the free end of the pipe are shown in Fig. 8.

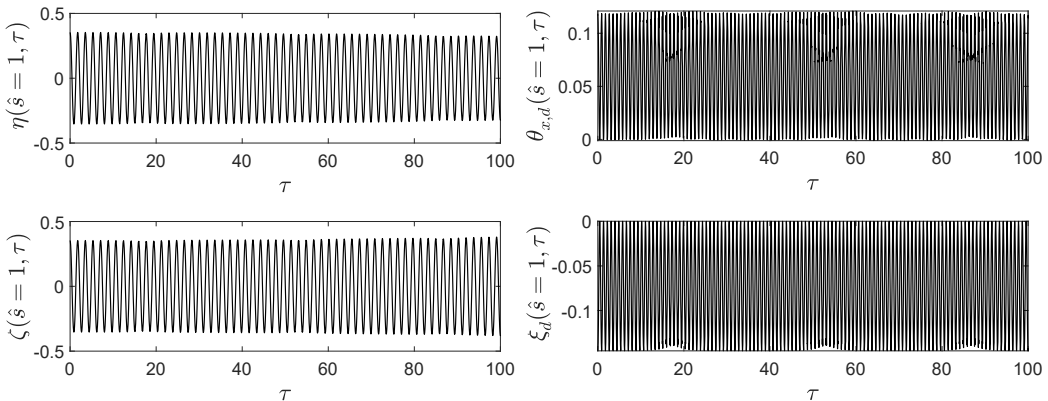


Figure 8: Free and undamped vibrations scenario where the pipe remains in a vertical plane inclined 45° with respect to the y - and z -axes.

As shown in Fig. 8, both transverse displacements $\eta(\hat{s} = 1, \tau)$ and $\zeta(\hat{s} = 1, \tau)$ are synchronous and thus the motion remains in the vertical plane described above. It is intuitive that, in the scenario depicted in Fig. 8, the real torsion along the pipe must be zero. Accordingly, since η and ζ change with time, then so must $\theta_{x,d}$ such that Eq. (28) is equal to zero. In Figs. 9 (a), the real dynamical torsional angle θ_d is shown both as a function of \hat{s} and at $\tau = 60.1$, when a maximum amplitude occurs, and at the free end of the pipe along the whole simulation time.

As is shown in Fig. 9, the real torsional angles are negligible and, within $0 < \tau < 100$, reach maximum values of the order of 10^{-3} . Fig. 9 (b), in turn,

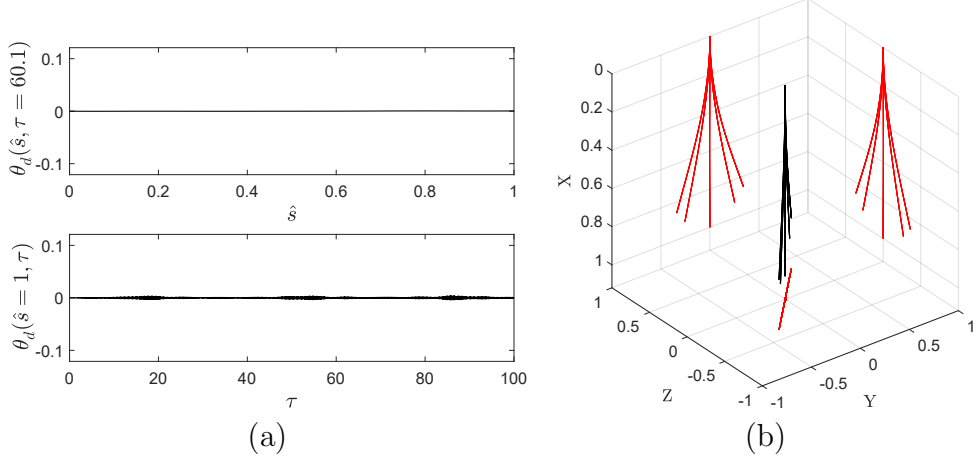


Figure 9: Plots showing (a) the real dynamical torsional angles and (b) five snapshots of the planar configuration of the pipe (black lines), as well as their projections in the (x, y) -, (x, z) - and (y, z) -planes (red lines), which are equally distributed along half of the period of oscillations.

shows five snapshots of the planar configuration of the pipe (black lines), as well as their projections in the (x, y) -, (x, z) - and (y, z) -planes (red lines), which are equally distributed along half of the period of oscillations.

This shows that the asymmetries discussed in this section are mathematical asymmetries due to how the kinematics of the system is formulated and described. The inextensibility and no-real-torsion shapes described in Sec. 3.2 are essential to obtain the behavior depicted in Fig. 8. If excessive initial strain energy is not prevented, then the movement of the pipe becomes erratic and tridimensional, even in the first period of oscillations.

4. Results and discussions

This section contains results obtained using the present mathematical model. Firstly, the capacity of the ROM in representing the stability conditions for pipes conveying fluid, with respect to the internal flow, is addressed, allowing for a choice on the number of shape functions N_T to be made. Then, as a benchmark for the present model, stability curves for horizontal and vertical pipes obtained using the present model and others found in the literature are compared. Finally, the effects of the applied torsional moment on the stability of the pipe are first characterized without the presence of internal flow. Then, the effects of said torsional moment on the stability conditions of the

pipe are studied, for two different placement positions. Unless when otherwise specified, across all results shown in this section, the parameters kept fixed are $\kappa_1 = 2$, $\kappa_3 = 0.7$, $\kappa_4 = 0.001$, $\kappa_5 = 0.001$, $N_{as} = N_{rs} = 4$, $N_a = 3$, $N_r = 4$ and $N_t = 8$. Additionally, the dimensionless axial stiffness parameter κ_2 is kept at 10000 in order to provide a near-inextensibility behavior to the pipe.

Shown in Fig. 10 is the capacity of the ROM in reproducing the stability conditions of a horizontal pipe with respect to the internal flow velocity as a function of the mass-ratio parameter β , as well as the number of shape functions N_t used in discretizing the transverse displacements.

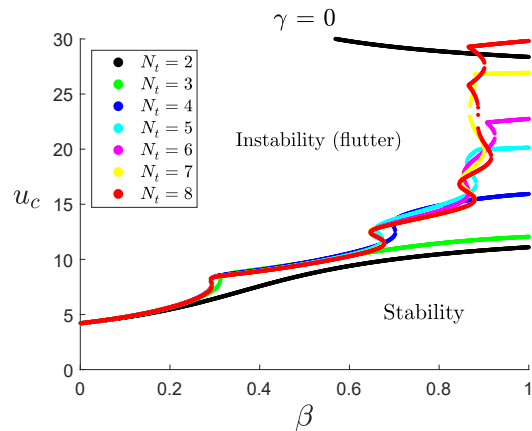


Figure 10: Critical flow velocities obtained using the present model, as a function of β and the number of transverse shape functions used in the Galerkin's discretization, while $N_a = 3$ and $N_r = 4$.

As Fig. 10 shows, and as is well known in the literature (e.g. in [22]), the problem of pipes conveying fluid is very demanding on the ROM in terms of correctly representing its dynamical features, even when considering inherently linear stability analyses. This need to use a fairly high number of transverse shape functions increases as the value for β increases. Physically, given that β represents a mass ratio between the fluid mass with respect to the overall mass of the system, this means that modeling pipes conveying air ($\cong \beta = 0.001$, see [8]) is significantly less demanding on the ROM than pipes conveying heavier fluids, such as water ($\cong \beta = 0.6$, see [25]).

Additionally, a well-known feature of the $u_c \times \beta$ stability curves for pipes conveying fluid is the existence of regions where restabilization can be achieved by increasing the internal flow velocity. For example, this phe-

nomenon occurs when $\beta \cong 0.65$, given $N_t = 8$. This leads to sudden changes in the critical flow velocity as β is increased, commonly referred to in the literature by “jumps” in the critical flow velocities. As the author in [22] refers to this behavior of the $u_c \times \beta$ stability curves with respect to β and the number of transverse shape functions, “each jump is associated with the addition of another generalized coordinate, while the approximation prior to the jump is quite reasonable without it”. As mentioned in the beginning of this section, and for this reason, 8 transverse shape function are used in generating every result shown from here on.

Now, for the purpose of benchmarking the current model, the results concerning the critical flow velocities obtained using the present model are compared to the ones obtained using other models found in the literature. Firstly, consider Fig. 11 (a), which shows a comparison between the critical flow velocities as a function of β using the present model and the 2D linear mathematical model for an inextensible and horizontal pipe published in [7].

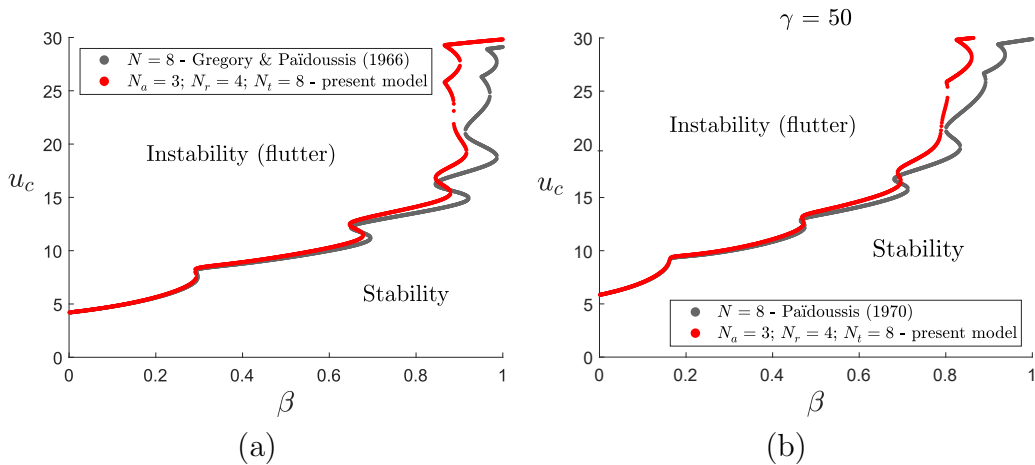


Figure 11: Comparison between the critical flow velocities as function of β obtained using (a) the present model (red line) and the model published in [7] (grey line); (b) the present model (red line) and the model published in [8] (grey line), with $\gamma = 50$.

Given that extensibility is inherent to the present mathematical model, a few key differences are seen in Fig. 11 (a), even with a fairly high value of κ_2 granting the pipe a near-inextensibility behavior. As discussed in [10], the critical flow velocities are slightly larger when compared to those of inextensible pipes. Moreover, it is well known in the literature that the dimensionless critical flow velocities increase with an increase in the mass-ratio parame-

ter β . Consequently, the differences in the critical flow velocities between both models are shown to be larger as β increases. A similar comparison is made between stability curves obtained using the present model and the linear mathematical model for a vertical and inextensible pipe published in [8] (see Fig. 11 (b)). Also in this case, differences related to the fact that the pipe is extensible can be seen, and the same observations made in the horizontal case apply in this case. Moreover, as expected, the critical flow velocities for a vertical pipe are higher than those of a horizontal pipe due to the additional gravitational restoring force.

These increases in the critical flow velocities due to the fact that the pipe is extensible become larger as the axial stiffness of the pipe is decreased, i.e. when lower values of κ_2 are considered. In Fig. 12, the axial stiffness parameter κ_2 is set to 5000, i.e. the axial stiffness is halved when compared to the pipe considered in Fig. 11 (a). As is shown, the effects of lowering κ_2 from 10000 to 5000 are only quantitative, and the critical flow velocities are once again slightly increased as a result.

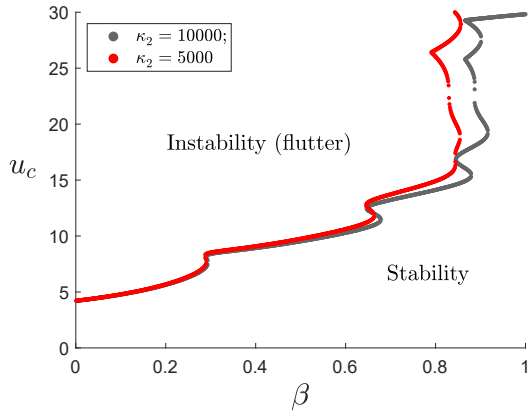


Figure 12: Comparison between the critical flow velocities for extensible pipes as function of β obtained using $\kappa_2 = 10000$ (grey curve) and $\kappa_2 = 5000$ (red curve).

As discussed in Sec. 1, while models for 3D extensible pipes have been published previously, to the best of the author's knowledge, no models for pipes conveying fluid which includes the torsional dynamics exist yet. The rest of this section is dedicated to characterizing the effects of torsion on the dynamics and stability of pipes conveying fluid obtained using the present model.

Initially, before focusing on the aforementioned effects on the stability

with respect to the internal flow and internal-flow-related dynamics of the pipe, the effects of torsion on the plain pipe, as a structural element, must be addressed. The fact that torsion may induce the occurrence of divergence (i.e. static instability) in beams, if above a certain critical value, has been reported in the literature (see, for example, [26], [27] and [28]). While the qualitative conclusions drawn in those works are in agreement with what is observed in the present model, as is discussed further on in this section, when it comes to quantitative comparisons, a few key points must be mentioned.

The first one is that the modelings conducted in the present work and in [26], [27] and [28] are fundamentally different in terms of the hypotheses made. More specifically, in those works, the torsional angular displacements are considered to be small when compared to the transverse ones. In the present work, as discussed in Sec. 2.1, the magnitude of every displacement field is considered to be equal, with the exception of the axial displacements. Moreover, in the works mentioned above, only the equilibrium of the bending moments along the beam is characterized as a function of the applied torsional moment, which is decomposed in each transverse direction. In the present work, both bending and torsional moment equilibria along the beam are considered in the analyses presented, as presented in Sec. 2. Consequently, while the effects of the torsional angles on the bending moment equilibrium are neglected in the works found in the literature, they are considered in the present modeling. This implies on the critical value for the torsional moment, in the references above, being independent of the torsional stiffness, whereas it is influenced by it in the present model.

The critical value for the dimensionless localized torsional moment, denoted by $\kappa_{0,c}$, as a function of the application point $\bar{\xi}_T$, is shown in Fig. 13.

Thus, if a torsional moment of $\kappa_0 > \kappa_{0,c} \cong 0.76\pi$ is applied at the free end of the pipe, the straight equilibrium configuration loses stability via divergence and, upon any disturbances, the pipe moves away from it and rests in a new 3D equilibrium position. For the middle point of the pipe, on the other hand, $\kappa_{0,c} \cong 1.49\pi$ and, as is seen in Fig. 13, as the application point moves away from the free end and closer to the support, the critical value for the torsional moment increases considerably. Yet more, as is seen from the figure, this increase does not occur in a linear manner.

Now, the effects of torsional moments on the critical flow velocities of the pipe conveying fluid are analysed. Two placement positions are considered, namely the free end of the pipe ($\bar{\xi}_T = 1.0$) and at its middle point ($\bar{\xi}_T = 0.5$).

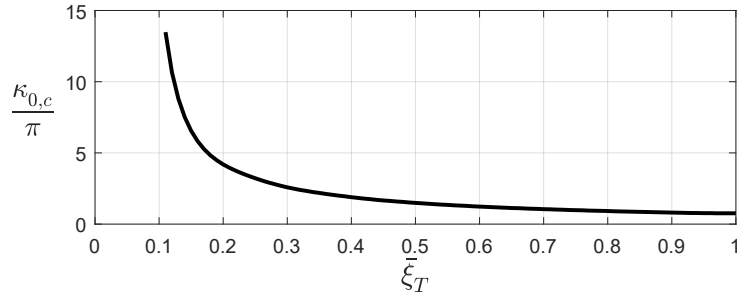


Figure 13: Critical torsional moment as a function of the placement position along the length of the pipe. Above these critical values, the torsional moment induces divergence in the pipe.

For each one, two values for the torsional moment are considered: one slightly below its critical value, and one considerably above, being approximately two times the critical value. Consider first the torsional moment application at the free end of the pipe, which leads to the stability curves shown in Fig. 14.

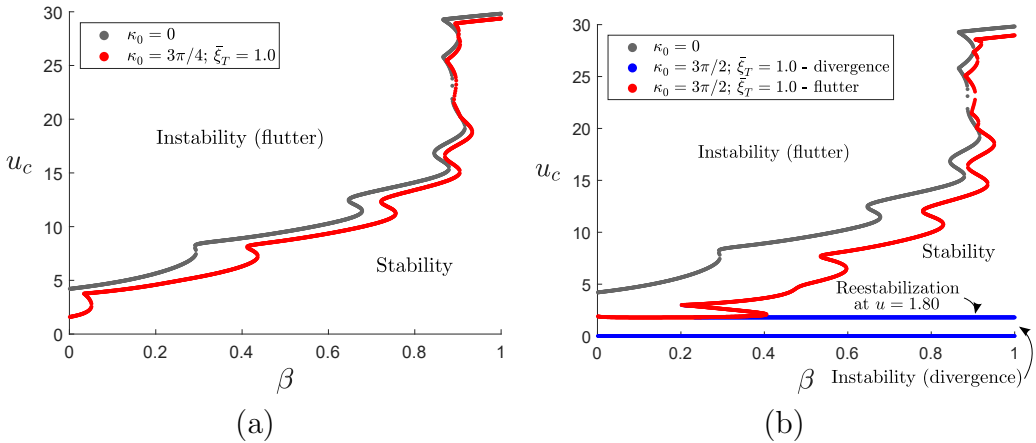


Figure 14: Critical flow velocities for a horizontal pipe with a torsional moment of magnitude (a) $\kappa_0 = 3\pi/4 < \kappa_{0,c}$ and (b) $\kappa_0 = 3\pi/2 > \kappa_{0,c}$ applied at its free end (red curve). The critical flow velocities for the system without the addition of a torsional moment is also shown (grey curve).

When $\kappa_0 = 3\pi/4$ (see Fig. 14 (a)), since the value for the torsional moment is below the critical value, no divergence is seen to occur. This leads to a qualitatively similar scenario, where the straight configuration of the pipe is stable, if the flow velocity is below the critical value, and unstable via a

Hopf bifurcation, if above. However, the impact of this application on the critical flow velocities of the pipe are considerable. Across all values of β , the critical flow velocities are smaller when compared to the system with no applied torsional moment, and this reduction is relatively more severe for lower values of β . Therefore, while pipes conveying water are slightly destabilized, flutter may occur on pipes conveying air for internal flow velocities as low as 38% of its original value.

When $\kappa_0 = 3\pi/2$ (see Fig. 14 (b)), on the other hand, since the value for κ_0 is above its critical value, the straight equilibrium configuration is unstable, when $u = 0$. As the internal flow velocity is increased, depending on the value of β , two scenarios may occur. For pipes with $\beta \lesssim 0.23$, increasing the flow velocity above the critical value leads to flutter. This occurs because the critical flow velocity above which flutter occurs is smaller than the flow velocity needed to restabilize the pipe under divergence. When $\beta \gtrsim 0.23$, in turn, the straight equilibrium configuration of the pipe is stable if $1.80 < u < u_c$. While the internal flow velocity which leads to a reestabilization does not depend on β , the critical flow velocity does. If the flow rate is increased above the critical value, which is now lower than when $\kappa_0 = 0$ or $\kappa_0 = 3\pi/4$, flutter occurs. Also in this case, the critical flow velocities are more intensely reduced for lower values of β , which indicates that this effect is related to the placement position, not the magnitude of the torsional moment.

Now, the same analysis is made when torsional moments are applied at the middle point of the pipe. Firstly, consider Fig. 15 (a), which shows the effects of a subcritical torsional moment of value $\kappa_0 = 1.45\pi$ on the critical flow velocities of the pipe conveying fluid.

Similarly as when the subcritical addition is made at the free end of the pipe, the flow velocities are reduced across all values of β , but no divergence is seen to occur. However, one key difference is seen between additions made at the free end and at the middle point of the pipe. Now, while pipes conveying air have their critical flow velocities slightly reduced, pipes conveying heavier fluids may experience flutter for significantly lower flow velocities. Notice that, for very high values of β , the flow velocities may be reduced to as low as 35% of its original value, prior to the torsional moment addition.

When a postcritical torsional moment of value $\kappa_0 = 3\pi$ is added at the middle point of the pipe (Fig. 15 (b)), in turn, the same qualitative behavior is seen when compared to the postcritical free end addition. When $u = 0$, divergence occurs on the pipe and, if the flow velocity is increased to $u = 3.46$, reestabilization can be achieved, but only for pipes with $\beta \gtrsim 0.08$, for which

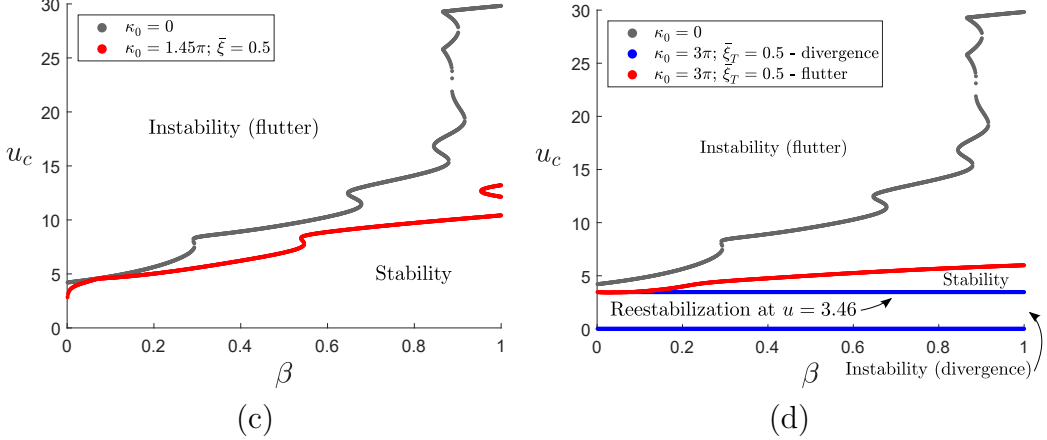


Figure 15: Critical flow velocities for a horizontal pipe with a torsional moment of magnitude (a) $\kappa_0 = 1.45\pi < \kappa_{0,c}$ and (b) $\kappa_0 = 3\pi > \kappa_{0,c}$ applied at its middle point (red curve). The critical flow velocities for the system without the addition of a torsional moment is also shown (grey curve).

the critical flow velocity is above 3.46. When $\beta \lesssim 0.08$, flutter takes place before the reestablishment can be achieved due to the critical flow velocities being smaller than 3.46.

For scenarios in which a postcritical torsional moment is applied at the free end of the pipe, the dynamical features described above are further inspected using root-loci plots of the lowest frequency modes of the system. Thus, the root-loci presented represent vertical lines in the stability curve shown in Fig. 14 (b), as u is increased.

Considering a pipe with $\beta = 0.1$, in which the critical flow velocity is lower than the necessary value to restabilize the straight configuration of the pipe, the associated root-locus is shown in Fig. 16 (a). As is shown, when $u = 0$, the maximum $\Re(\lambda)$ is positive, meaning that static instability occurs. When $0 < u < 1.75$, this maximum value is lowered, but is still positive, and no eigenvalues with positive real part and nonzero imaginary part exist. When $1.75 < u < 1.80$, flutter and divergence are seen to coexist and, finally, when $u > 1.80$, the system is only subject to flutter.

Now considering a pipe with $\beta = 0.7$, in which reestablishment due to the internal flow is seen possible, the resultant root-locus is shown in Fig. 16 (b). In this case, when $0 < u < 1.80$, the system is only subject to divergence. When $1.80 < u < 8.92$, in turn, no eigenvalues with positive real part are

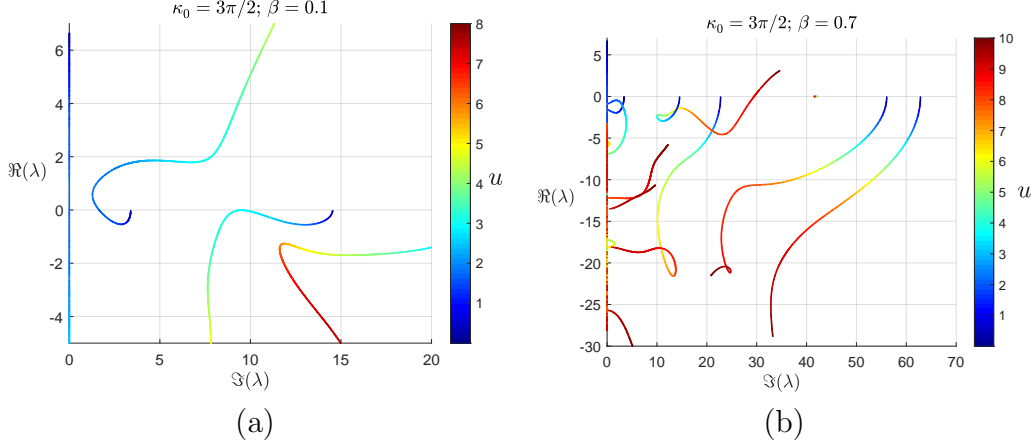


Figure 16: Root loci of the lowest-frequency modes of the system when $\kappa_0 = 3\pi/2 > \kappa_{0,c}$, (a) $\beta = 0.1$ and (b) $\beta = 0.7$.

seen, and thus the straight equilibrium configuration of the pipe is stable. Then, for internal flow velocities higher than 8.92, dynamic instability takes place.

An unexpected analogy can be drawn between these dynamical features and the ones obtained when considering standing discharging pipes, i.e. pipes with a negative value of γ and thus that discharge fluid in an opposite direction with respect to gravity. As discussed in Sec. 1, standing pipes may experience divergence if the absolute value of γ is exceedingly high. If the flow velocity is increased, flutter and divergence may coexist or not, depending on the parameters of the system. These theoretical observations were experimentally verified in [8], where the author mentions this capacity of the system to be “stabilized by flow”. These internal-flow induced effects are very similar to the ones shown in this section, despite the fact that the static instabilities now arise from excessive localized torsional moment applications.

To analyse the dynamical behavior of the system in scenarios characterized by different points in Fig. 16 (b), this section is concluded by presenting time series for the displacements of the free end of the pipe. This is done by numerically integrating the EOM shown in Eqs. (79)-(82) while considering $B_1 = 0.001$ and $A_3 = 1$ (corresponding to the inextensibility shape described in Sec. 3) as the only nontrivial initial conditions.

The first scenario considered is when the internal flow velocity is lower than the one necessary in order to restabilize the system. For $u = 0.5 < u_c$,

the associated time series for ξ_d , η , ζ and $\theta_{x,d}$ are shown in Fig. 17.

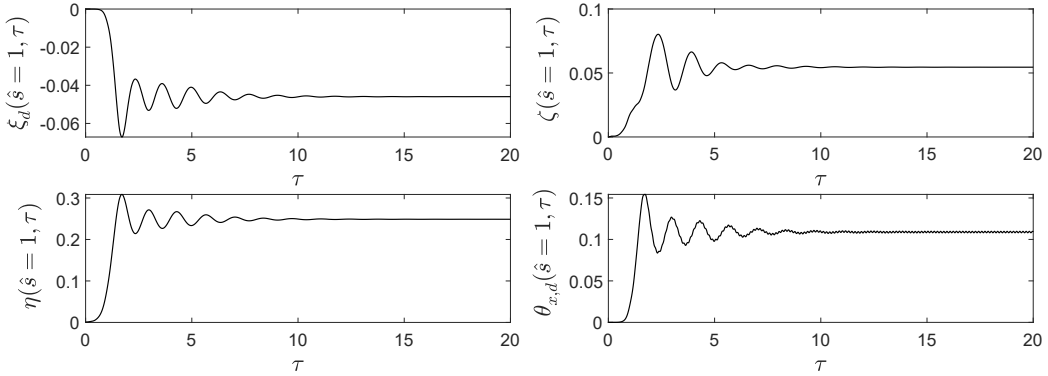


Figure 17: Time series obtained by numerically integrating the EOM of the mathematical model using $u = 0.5 < u_c$.

Given the applied postcritical torsional moment, the pipe moves away from the unstable straight equilibrium configuration and oscillates around a new stable equilibrium configuration. Due to the internal-flow-induced damping, in the steady state regime, the pipe rests in this new configuration. It is worth noting that, although a 2D initial configuration is given to the system, the new equilibrium configuration is 3D due to the applied torsional moment (see Fig. 18).

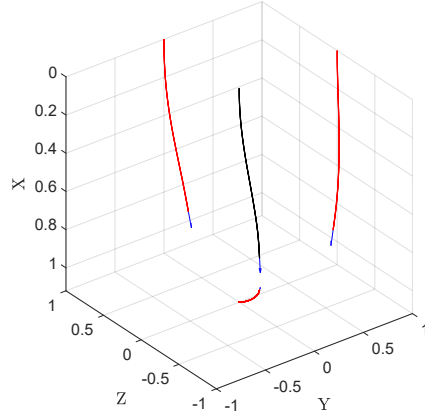


Figure 18: New stable 3D equilibrium configuration when an internal flow velocity of $u = 0.5 < u_c$ is considered.

Now, consider a scenario in which the internal flow velocity is high enough

to inhibit the occurrence of divergence, but not to induce flutter. The resultant simulation when an internal flow velocity $u = 5 < u_c$ is used is shown in Fig. 19.

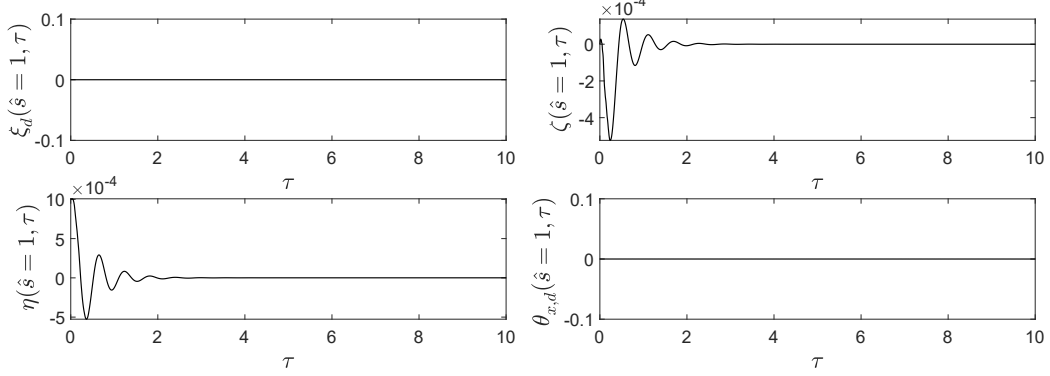


Figure 19: Time series obtained by numerically integrating the EOM of the mathematical model using $u = 5 < u_c$.

In this case, since the internal flow restabilized the system, the straight equilibrium configuration is stable and, due to the internal-flow-induced damping, the system rests in it in the steady state regime.

The last scenario shown is one in which the internal flow velocity is above the critical value. Given the value of β , if the value is high enough to induce flutter, then divergence no longer occurs. Results obtained when $u = 10 > u_c$ are shown in Fig. 20.

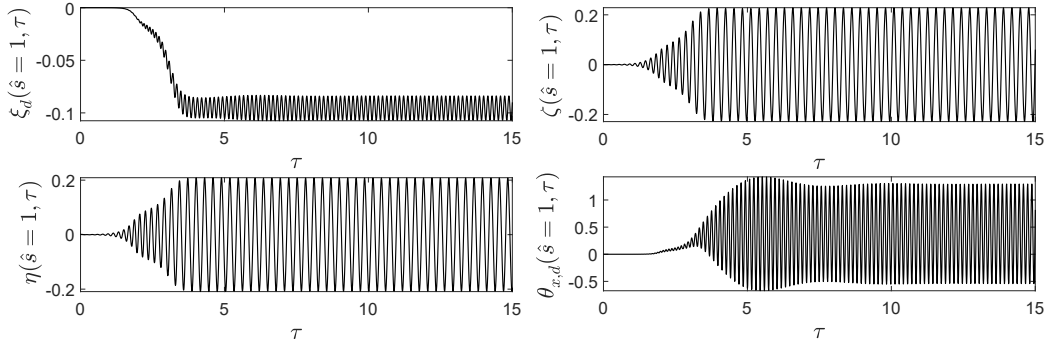


Figure 20: Time series obtained by numerically integrating the EOM of the mathematical model using $u = 10 > u_c$.

As expected, given the postcritical internal flow velocity used, the pipe

moves away from the straight equilibrium configuration, in an oscillatory manner, and, after an initial transient regime, achieves an postcritical limit cycle in which the amplitudes of oscillation are approximately constant. Also in this case, although planar initial conditions were given, the limit cycle is 3D due to the nonlinear coupling related to the torsional moment applied at the free end of the pipe (see Fig. 21 (b)). Lastly, still considering the case in which $u = 10$, the real torsional angles are shown, in Figs. 21 (a), both as a function of \hat{s} , when $\tau = 8.8$ (when θ_d is maximum in the steady state regime), and at the free end of the pipe along the whole simulation shown.

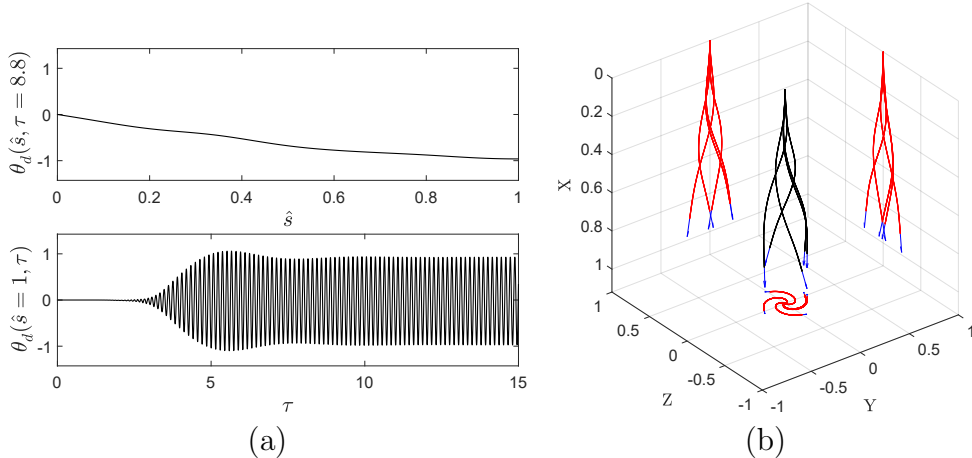


Figure 21: Plots showing (a) the real dynamical torsional angles and (b) five snapshots of the planar configuration of the pipe (black lines), as well as their projections in the (x, y) -, (x, z) - and (y, z) -planes (red lines), which are equally distributed along one period of oscillations. The direction of the discharging fluid is shown using a blue arrow at the free end of the pipe.

As can be seen in Figs. 21 (a), in the steady state regime, the torsional angles can be considerable, reaching maximum amplitudes of around 45° at the free end of the pipe.

5. Conclusions

In the present work, a 3D and nonlinear mathematical model for a cantilevered pipe conveying fluid was derived and presented. The nonlinearities were expanded up to cubic order and the axial and torsional dynamics were also included in the modeling. The axial and torsional static solutions were

numerically evaluated while considering the nonlinear coupling between both displacement fields. The dynamics of the system was subsequently formulated around these static solutions and, for determining both the static and dynamical solutions, the Galerkin's method was used. While polynomial shape functions were used in determining the static solutions, modal shapes were used when approximations for the dynamical solutions were sought. To study the effects of torsional moments on the dynamics and stability of the pipe conveying fluid, a localized torsional moment was applied at a point along the length of the pipe. The consideration of extensibility in the modeling of the pipe led to slightly higher critical flow velocities when compared to inextensible pipes. This increase was shown to be higher as the axial stiffness of the pipe was reduced. When the fluid inside the pipe is still, its straight equilibrium configuration may lose stability via divergence if the applied torsional moment is above the critical value. The critical value for the torsional moments was characterized as a function of the application point, and it was shown that it becomes nonlinearly higher as the application point nears the supported inlet point. The effects of the torsional moment application on the fluid-related stability of the pipe were characterized for when the application point is the middle and free end points of the pipe. The critical flow velocities were shown to be reduced upon the application of the torsional moment, in both cases. Additionally, it was shown that pipes characterized by smaller values of β , such as ones conveying air, are more destabilized by free end applications. The stability of pipes characterized by higher values of β , such as when water is conveyed, is more sensitive to torsional moments applied at the middle point. When postcritical torsional moments were considered and for both application points, the internal flow was shown to restabilize the divergence induced by the torsional moment for pipes with higher values of β . In such cases, divergence and flutter were shown to not coexist. For pipes with lower values of β , in turn, divergence and flutter may occur for a narrow range of internal flow velocities. By numerically integrating the EOM, the dynamical response of the pipe was studied for some of the scenarios mentioned above. It was shown that the nonlinear coupling related to the applied torsional moment induced 3D motions in cases where the initial configuration was 2D. In such scenarios, and when no torsional moments are applied to the pipe, the motions exhibited by the pipe are always 2D.

Acknowledgments

The first author is thankful to FAPESP for his PhD scholarship (grant number 2021/04434-1) and for the research internship scholarship at Concordia University (grant number 2022/12546-7). **Other acknowledgements...**

References

- [1] M. P. Païdoussis, G. X. Li, Pipes conveying fluid: A model dynamical problem, *Journal of Fluids and Structures* 7 (1992) 137–204. doi:10.1006/jfls.1993.1011.
- [2] M. P. Païdoussis, Pipes conveying fluid: A fertile dynamics problem, *Journal of Fluids and Structures* 114 (2022) 103664. doi:<https://doi.org/10.1016/j.jfluidstructs.2022.103664>.
- [3] T. B. Benjamin, Dynamics of a system of articulated pipes conveying fluid. I. Theory, *Proceedings of the Royal Society* 261 (1961) 457–486.
- [4] D. B. McIver, Hamilton’s principle for systems of changing mass, *Journal of Engineering Mathematics* 7 (1973) 249–261.
- [5] L. Casetta, C. P. Pesce, The generalized Hamilton’s principle for a non-material volume, *Acta Mechanica* 224 (2013) 919–924. doi:10.1007/s00707-012-0807-9.
- [6] M. Kheiri, M. P. Païdoussis, On the use of generalized Hamilton’s principle for the derivation of the equation of motion of a pipe conveying fluid, *Journal of Fluids and Structures* 50 (2014) 18–24. doi:10.1016/j.jfluidstructs.2014.06.007.
- [7] R. W. Gregory, M. P. Païdoussis, Unstable oscillation of tubular cantilevers conveying fluid. I. Theory, *Proceedings of the Royal Society* 293 (1966) 512–527.
- [8] M. P. Païdoussis, Dynamics of tubular cantilevers conveying fluid, *Journal of Mechanical Engineering Science* 12 (1970) 85–103. doi:10.1243/JMES.
- [9] C. Semler, G. X. Li, M. P. Païdoussis, The non-linear equations of motion of pipes conveying fluid, *Journal of Sound and Vibration* 169 (1992) 577–599.

- [10] M. H. Ghayesh, M. P. Païdoussis, Three-dimensional dynamics of a cantilevered pipe conveying fluid, additionally supported by an intermediate spring array, *International Journal of Non-Linear Mechanics* 45 (2010) 507–524.
- [11] H. Irschik, H. J. Holl, The equations of Lagrange written for a non-material volume, *Acta Mechanica* 153 (2002) 231–248. doi:10.1007/BF01177454.
- [12] M. Wadham-Gagnon, M. P. Païdoussis, C. Semler, Dynamics of cantilevered pipes conveying fluid. Part 1: Nonlinear equations of three-dimensional motion, *Journal of Fluids and Structures* 23 (2006) 545–567.
- [13] Y. Modarres-Sadeghi, M. P. Païdoussis, C. Semler, Three-dimensional oscillations of a cantilevered pipe conveying fluid, *International Journal of Non-Linear Mechanics* 43 (2007) 18–25. doi:doi:10.1016/j.ijnonlinmec.2007.09.005.
- [14] A. Askarian, M. Kheiri, Three-dimensional nonlinear dynamics of an extensible pipe conveying fluid, in: 9th International Symposium on Fluid-Structure Interactions, Flow-Sound Interactions, Flow-Induced Vibration & Noise, 2018.
- [15] H. Farokhi, M. Tavallaeinejad, M. P. Païdoussis, Geometrically exact dynamics of cantilevered pipes conveying fluid, *Journal of Fluids and Structures* 106 (2021) 103364. doi:<https://doi.org/10.1016/j.jfluidstructs.2021.103364>.
- [16] W. Chen, H. Dai, Q. Jia, Geometrically exact equation of motion for large-amplitude oscillation of cantilevered pipe conveying fluid, *Nonlinear Dynamics* 98 (2019) 2097–2114. doi:<https://doi.org/10.1007/s11071-019-05310-0>.
- [17] W. Chen, H. Dai, L. Wang, Three-dimensional dynamical model for cantilevered pipes conveying fluid under large deformation, *Journal of Fluids and Structures* 105 (2021) 103329. doi:<https://doi.org/10.1016/j.jfluidstructs.2021.103329>.
- [18] R. M. M. Orsino, C. P. Pesce, Reduced order modeling of a cantilevered pipe conveying fluid applying a modular methodology,

International Journal of Non-Linear Mechanics 103 (2018) 1–11.
doi:10.1016/j.ijnonlinmec.2018.04.003.

- [19] A. Sarkar, M. P. Païdoussis, A compact limit-cycle oscillation model of a cantilever conveying fluid, *Journal of Fluids and Structures* 17 (2003) 525–539. doi:[https://doi.org/10.1016/S0889-9746\(02\)00150-0](https://doi.org/10.1016/S0889-9746(02)00150-0).
- [20] M. Li, H. Yan, L. Wang, Nonlinear model reduction for a cantilevered pipe conveying fluid: a system with asymmetric damping and stiffness matrices, *Mechanical systems and signal processing* 188 (2023) 109993. doi:<https://doi.org/10.1016/j.ymssp.2022.109993>.
- [21] M. Li, H. Yan, L. Wang, Data-driven model reduction for pipes conveying fluid via spectral submanifolds, *International Journal of Mechanical Sciences* 188 (2023) 109414.
- [22] M. P. Païdoussis, *Fluid-Structure Interactions: Slender Structures and Axial Flow*, Academic Press, 2014.
- [23] M. R. M. Crespo da Silva, Non-linear flexural-flexural-torsional-extensional dynamics of beams — I. Formulation, *International Journal of Solids and Structures* 24 (1988) 1225–1234.
- [24] C. Truesdell, R. A. Toupin, *The classical field theories*, Berlin: Springer, 1960.
- [25] R. W. Gregory, M. P. Païdoussis, Unstable oscillation of tubular cantilevers conveying fluid. II. Experiments, *Proceedings of the Royal Society* 293 (1966) 528–542.
- [26] A. G. Greenhill, On the strength of shafting when exposed both to torsion and to end thrust, *Proceedings of the Institution of Mechanical Engineers* 34 (1) (1883) 182–225.
- [27] Z. P. Bazant, L. Cedolin, *Stability of Structures: Elastic, Inelastic, Fracture, and Damage Theories*, 2003.
- [28] H. Ziegler, *Principles of Structural Stability*, Birkhäuser Basel, 1977. doi:10.1007/978-3-0348-5912-7.

Appendix A. Explicit expressions for the tensors $\mathbf{V}^{(1)} - \mathbf{V}^{(62)}$

$$\mathbf{V}^{(1)}(k, n) = - \int_0^1 \phi_n \phi_k d\hat{s}, \quad (\text{A.1})$$

for $k = 1, \dots, N_a$ and $n = 1, \dots, N_a$,

$$\mathbf{V}^{(2)}(k, n) = -\sqrt{\beta} u \phi_{n,1} \phi_{k,1}, \quad (\text{A.2})$$

for $k = 1, \dots, N_a$ and $n = 1, \dots, N_a$,

$$\mathbf{V}^{(3)}(k, n) = \kappa_2 \int_0^1 \phi_n'' \phi_k d\hat{s} - \kappa_2 \phi_{n,1}' \phi_{k,1}, \quad (\text{A.3})$$

for $k = 1, \dots, N_a$ and $n = 1, \dots, N_a$,

$$\begin{aligned} \mathbf{V}^{(4)}(k, n) = & \kappa_1 \int_0^1 (\theta'_{x,s} \Theta'_n)' \phi_k d\hat{s} - \kappa_1 \theta'_{x,s,1} \Theta'_{n,1} \phi_{k,1} - \\ & - \kappa_1 \theta'_{x,s,\bar{\xi}_-} \Theta'_{n,\bar{\xi}_-} \phi_{k,\bar{\xi}_-} + \kappa_1 \theta'_{x,s,\bar{\xi}_+} \Theta'_{n,\bar{\xi}_+} \phi_{k,\bar{\xi}_+}, \end{aligned} \quad (\text{A.4})$$

for $k = 1, \dots, N_a$ and $n = 1, \dots, N_r$,

$$\begin{aligned} \mathbf{V}^{(5)}(k, n, m) = & \frac{\kappa_2}{2} \int_0^1 (\psi'_n \psi'_m)' \phi_k d\hat{s} - 2 \int_0^1 \psi''_n \psi'''_m \phi_k d\hat{s} + \int_0^1 (\psi''_n \psi'_m)'' \phi_k d\hat{s} - \\ & - \frac{\kappa_2}{2} \psi'_{n,1} \psi'_{m,1} \phi_{k,1} + \psi''_{n,1} \psi''_{m,1} \phi_{k,1} - (\psi''_n \psi'_m)'|_{\hat{s}=1} \phi_{k,1} + \frac{u^2}{2} \psi'_{n,1} \psi'_{m,1} \phi_{k,1} + \\ & + \psi'_{n,1} \psi''_{m,1} \phi'_{k,1}, \end{aligned} \quad (\text{A.5})$$

for $k = 1, \dots, N_a$, $n = 1, \dots, N_t$ and $m = 1, \dots, N_t$,

$$\begin{aligned}
\mathbf{V}^{(6)}(k, n, m) = & \frac{\kappa_2}{2} \int_0^1 (\psi'_n \psi'_m)' \phi_k d\hat{s} - 2 \int_0^1 \psi''_n \psi'''_m \phi_k d\hat{s} + \int_0^1 (\psi''_n \psi'_m)'' \phi_k d\hat{s} - \\
& - \frac{\kappa_2}{2} \psi'_{n,1} \psi'_{m,1} \phi_{k,1} + \psi''_{n,1} \psi''_{m,1} \phi_{k,1} - (\psi''_n \psi'_m)'|_{\hat{s}=1} \phi_{k,1} + \frac{u^2}{2} \psi'_{n,1} \psi'_{m,1} \phi_{k,1} + \\
& + \psi'_{n,1} \psi''_{m,1} \phi'_{k,1}, \tag{A.6}
\end{aligned}$$

for $k = 1, \dots, N_a$, $n = 1, \dots, N_t$ and $m = 1, \dots, N_t$,

$$\mathbf{V}^{(7)}(k, n, m) = \kappa_1 \int_0^1 \Theta'_n \Theta''_m \phi_k d\hat{s} - \frac{\kappa_1}{2} \Theta'_{n,1} \Theta'_{m,1} \phi_{k,1}, \tag{A.7}$$

for $k = 1, \dots, N_a$, $n = 1, \dots, N_r$ and $m = 1, \dots, N_r$,

$$\begin{aligned}
\mathbf{V}^{(8)}(k, n, m) = & -\kappa_1 \int_0^1 (\theta'_{x,s} \psi'_n \psi''_m)' \phi_k d\hat{s} - \int_0^1 (\theta_{x,s} \psi''_n \psi'_m)'' \phi_k d\hat{s} + \\
& + \int_0^1 (\theta_{x,s} \psi'_n \psi''_m)'' \phi_k d\hat{s} + \kappa_1 \theta'_{x,s,1} \psi'_{n,1} \psi''_{m,1} \phi_{k,1} + (\theta_{x,s} \psi''_n \psi'_m)'|_{\hat{s}=1} \phi_{k,1} - \\
& - (\theta_{x,s} \psi'_n \psi''_m)'|_{\hat{s}=1} \phi_{k,1} - \theta_{x,s,1} \psi''_{n,1} \psi'_{m,1} \phi'_{k,1} + \theta_{x,s,1} \psi'_{n,1} \psi''_{m,1} \phi'_{k,1} + \\
& + \kappa_1 \theta'_{x,s,\bar{\xi}_-} \psi'_{n,\bar{\xi}_-} \psi''_{m,\bar{\xi}_-} \phi_{k,\bar{\xi}_-} - \kappa_1 \theta'_{x,s,\bar{\xi}_+} \psi'_{n,\bar{\xi}_+} \psi''_{m,\bar{\xi}_+} \phi_{k,\bar{\xi}_+} + (\theta_{x,s} \psi''_n \psi'_m)'|_{\hat{s}=\bar{\xi}_-} \phi_{k,\bar{\xi}_-} - \\
& - (\theta_{x,s} \psi''_n \psi'_m)'|_{\hat{s}=\bar{\xi}_+} \phi_{k,\bar{\xi}_+} - (\theta_{x,s} \psi'_n \psi''_m)'|_{\hat{s}=\bar{\xi}_-} \phi_{k,\bar{\xi}_-} + (\theta_{x,s} \psi'_n \psi''_m)'|_{\hat{s}=\bar{\xi}_+} \phi_{k,\bar{\xi}_+} - \\
& - \theta_{x,s,\bar{\xi}_-} \psi''_{n,\bar{\xi}_-} \psi'_{m,\bar{\xi}_-} \phi'_{k,\bar{\xi}_-} + \theta_{x,s,\bar{\xi}_+} \psi''_{n,\bar{\xi}_+} \psi'_{m,\bar{\xi}_+} \phi'_{k,\bar{\xi}_+} + \theta_{x,s,\bar{\xi}_-} \psi'_{n,\bar{\xi}_-} \psi''_{m,\bar{\xi}_-} \phi'_{k,\bar{\xi}_-} - \\
& - \theta_{x,s,\bar{\xi}_+} \psi'_{n,\bar{\xi}_+} \psi''_{m,\bar{\xi}_+} \phi'_{k,\bar{\xi}_+}, \tag{A.8}
\end{aligned}$$

for $k = 1, \dots, N_a$, $n = 1, \dots, N_t$ and $m = 1, \dots, N_t$,

$$\begin{aligned}
\mathbf{V}^{(9)}(k, n, m) = & \sqrt{\beta} u \int_0^1 \psi'_n \psi'_m \phi_k d\hat{s} + \sqrt{\beta} u \int_0^1 (\psi_n \psi'_m)' \phi_k d\hat{s} - \\
& - \sqrt{\beta} u \psi_{n,1} \psi'_{m,1} \phi_{k,1}, \tag{A.9}
\end{aligned}$$

for $k = 1, \dots, N_a$, $n = 1, \dots, N_t$ and $m = 1, \dots, N_t$,

$$\begin{aligned} \mathbf{V}^{(10)}(k, n, m) = & \sqrt{\beta} u \int_0^1 \psi'_n \psi'_m \phi_k d\hat{s} + \sqrt{\beta} u \int_0^1 (\psi_n \psi'_m)' \phi_k d\hat{s} - \\ & - \sqrt{\beta} u \psi_{n,1} \psi'_{m,1} \phi_{k,1}, \end{aligned} \quad (\text{A.10})$$

for $k = 1, \dots, N_a$, $n = 1, \dots, N_t$ and $m = 1, \dots, N_t$,

$$\begin{aligned} \mathbf{V}^{(11)}(k, n, m, p) = & -\kappa_1 \int_0^1 (\psi'_n \psi''_m \Theta'_p)' \phi_k d\hat{s} - \int_0^1 (\psi''_n \psi'_m \Theta_p)'' \phi_k d\hat{s} + \\ & + \int_0^1 (\psi'_n \psi''_m \Theta_p)'' \phi_k d\hat{s} + \kappa_1 \psi'_{n,1} \psi''_{m,1} \Theta'_{p,1} \phi_{k,1} + \psi''_{n,1} \psi'_{m,1} \Theta_{p,1} \phi_{k,1} - \\ & - \psi'_{n,1} \psi''_{m,1} \Theta_{p,1} \phi_{k,1} - \psi''_{n,1} \psi'_{m,1} \Theta_{p,1} \phi'_{k,1} + \psi'_{n,1} \psi''_{m,1} \Theta_{p,1} \phi'_{k,1}, \end{aligned} \quad (\text{A.11})$$

for $k = 1, \dots, N_a$, $n = 1, \dots, N_t$, $m = 1, \dots, N_t$ and $p = 1, \dots, N_r$,

$$\mathbf{V}^{(12)}(k, n) = - \int_0^1 \psi_n \psi_k d\hat{s}, \quad (\text{A.12})$$

for $k = 1, \dots, N_t$ and $n = 1, \dots, N_t$,

$$\begin{aligned} \mathbf{V}^{(13)}(k, n) = & -2\sqrt{\beta} u \int_0^1 \psi'_n \psi_k d\hat{s} + \sqrt{\beta} u \int_0^1 \xi'_s \psi'_n \psi_k d\hat{s} + \\ & + \sqrt{\beta} u \int_0^1 (\xi'_s \psi_n)' \psi_k d\hat{s} - \sqrt{\beta} u \xi'_{s,1} \psi_{n,1} \psi_{k,1} - \sqrt{\beta} u \xi'_{s,\bar{\xi}_-} \psi_{n,\bar{\xi}_-} \psi_{k,\bar{\xi}_-} + \\ & + \sqrt{\beta} u \xi'_{s,\bar{\xi}_+} \psi_{n,\bar{\xi}_+} \psi_{k,\bar{\xi}_+}, \end{aligned} \quad (\text{A.13})$$

for $k = 1, \dots, N_t$ and $n = 1, \dots, N_t$,

$$\begin{aligned}
\mathbf{V}^{(14)}(k, n) = & \kappa_2 \int_0^1 (\xi'_s \psi'_n)' \psi_k d\hat{s} + \frac{\kappa_1}{2} \int_0^1 (\theta'^2_{x,s} \psi'_n)' \psi_k d\hat{s} - \int_0^1 (\xi''_s \psi''_n)' \psi_k d\hat{s} - \\
& - \int_0^1 \psi''' \psi_k d\hat{s} + 2 \int_0^1 (\xi'_s \psi''_n)'' \psi_k d\hat{s} + \int_0^1 (\xi''_s \psi'_n)'' \psi_k d\hat{s} - \kappa_2 \xi'_{s,1} \psi'_{n,1} \psi_{k,1} - \\
& - \frac{1}{2} \kappa_1 \theta'^2_{x,s,1} \psi'_{n,1} \psi_{k,1} + \xi''_{s,1} \psi''_{n,1} \psi_{k,1} + \psi'''_{n,1} \psi_{k,1} - 2 (\xi'_s \psi''_n)'|_{\hat{s}=1} \psi_{k,1} - \\
& - (\xi'_s \psi'_n)'|_{\hat{s}=1} \psi_{k,1} - u^2 \psi'_{n,1} \psi_{k,1} + u^2 \xi'_{s,1} \psi'_{n,1} \psi_{k,1} - \psi''_{n,1} \psi'_{k,1} + 2 \xi'_{s,1} \psi''_{n,1} \psi'_{k,1} + \\
& + \xi''_{s,1} \psi'_{n,1} \psi'_{k,1} - \kappa_2 \xi'_{s,\bar{\xi}_-} \psi'_{n,\bar{\xi}_-} \psi_{k,\bar{\xi}_-} + \kappa_2 \xi'_{s,\bar{\xi}_+} \psi'_{n,\bar{\xi}_+} \psi_{k,\bar{\xi}_+} - \frac{1}{2} \kappa_1 \theta'^2_{x,s,\bar{\xi}_-} \psi'_{n,\bar{\xi}_-} \psi_{k,\bar{\xi}_-} + \\
& + \frac{1}{2} \kappa_1 \theta'^2_{x,s,\bar{\xi}_+} \psi'_{n,\bar{\xi}_+} \psi_{k,\bar{\xi}_+} + \xi''_{s,\bar{\xi}_-} \psi''_{n,\bar{\xi}_-} \psi_{k,\bar{\xi}_-} - \xi''_{s,\bar{\xi}_+} \psi''_{n,\bar{\xi}_+} \psi_{k,\bar{\xi}_+} - 2 (\xi'_s \psi''_n)'|_{\hat{s}=\bar{\xi}_-} \psi_{k,\bar{\xi}_-} + \\
& + 2 (\xi'_s \psi''_n)'|_{\hat{s}=\bar{\xi}_+} \psi_{k,\bar{\xi}_+} - (\xi''_s \psi'_n)'|_{\hat{s}=\bar{\xi}_-} \psi_{k,\bar{\xi}_-} + (\xi''_s \psi'_n)'|_{\hat{s}=\bar{\xi}_+} \psi_{k,\bar{\xi}_+} + 2 \xi'_{s,\bar{\xi}_-} \psi''_{n,\bar{\xi}_-} \psi'_{k,\bar{\xi}_-} - \\
& - 2 \xi'_{s,\bar{\xi}_+} \psi''_{n,\bar{\xi}_+} \psi'_{k,\bar{\xi}_+} + \xi''_{s,\bar{\xi}_-} \psi'_{n,\bar{\xi}_-} \psi'_{k,\bar{\xi}_-} - \xi''_{s,\bar{\xi}_+} \psi'_{n,\bar{\xi}_+} \psi'_{k,\bar{\xi}_+}, \tag{A.14}
\end{aligned}$$

for $k = 1, \dots, N_t$ and $n = 1, \dots, N_t$,

$$\begin{aligned}
\mathbf{V}^{(15)}(k, n) = & -\kappa_3 \int_0^1 (\theta'_{x,s} \psi''_n)' \psi_k d\hat{s} + \kappa_3 \theta'_{x,s,1} \psi''_{n,1} \psi_{k,1} + \\
& + \kappa_3 \theta'_{x,s,\bar{\xi}_-} \psi''_{n,\bar{\xi}_-} \psi_{k,\bar{\xi}_-} - \kappa_3 \theta'_{x,s,\bar{\xi}_+} \psi''_{n,\bar{\xi}_+} \psi_{k,\bar{\xi}_+}, \tag{A.15}
\end{aligned}$$

for $k = 1, \dots, N_t$ and $n = 1, \dots, N_t$,

$$\begin{aligned}
\mathbf{V}^{(16)}(k, n, m) = & \kappa_2 \int_0^1 (\phi'_n \psi'_m)' \psi_k d\hat{s} - \int_0^1 (\phi''_n \psi''_m)' \psi_k d\hat{s} + 2 \int_0^1 (\phi'_n \psi''_m)'' \psi_k d\hat{s} + \\
& + \int_0^1 (\phi''_n \psi'_m)'' \psi_k d\hat{s} - \kappa_2 \phi'_{n,1} \psi'_{m,1} \psi_{k,1} + \phi''_{n,1} \psi''_{m,1} \psi_{k,1} - 2 (\phi'_n \psi''_m)'|_{\hat{s}=1} \psi_{k,1} - \\
& - (\phi''_n \psi'_m)'|_{\hat{s}=1} \psi_{k,1} + u^2 \phi'_{n,1} \psi'_{m,1} \psi_{k,1} + 2 \phi'_{n,1} \psi''_{m,1} \psi'_{k,1} + \phi''_{n,1} \psi'_{m,1} \psi'_{k,1}, \tag{A.16}
\end{aligned}$$

for $k = 1, \dots, N_t$, $n = 1, \dots, N_a$ and $m = 1, \dots, N_t$,

$$\mathbf{V}^{(17)}(k, n, m) = \kappa_1 \int_0^1 (\theta'_{x,s} \psi'_n \Theta'_m)' \psi_k d\hat{s} - \kappa_1 \theta'_{x,s,1} \psi'_{n,1} \Theta'_{m,1} \psi_{k,1} - \\ - \kappa_1 \theta'_{x,s,\bar{\xi}_-} \psi'_{n,\bar{\xi}_-} \Theta'_{m,\bar{\xi}_-} \psi_{k,\bar{\xi}_-} + \kappa_1 \theta'_{x,s,\bar{\xi}_+} \psi'_{n,\bar{\xi}_+} \Theta'_{m,\bar{\xi}_+} \psi_{k,\bar{\xi}_+}, \quad (\text{A.17})$$

for $k = 1, \dots, N_t$, $n = 1, \dots, N_t$ and $m = 1, \dots, N_r$,

$$\mathbf{V}^{(18)}(k, n, m) = -\kappa_3 \int_0^1 (\psi''_n \Theta'_m)' \psi_k d\hat{s} + \kappa_3 \psi''_{n,1} \Theta'_{m,1} \psi_{k,1}, \quad (\text{A.18})$$

for $k = 1, \dots, N_t$, $n = 1, \dots, N_t$ and $m = 1, \dots, N_r$,

$$\mathbf{V}^{(19)}(k, n, m) = \sqrt{\beta} u \int_0^1 \phi'_n \psi'_m \psi_k d\hat{s} + \sqrt{\beta} u \int_0^1 (\phi_n \psi'_m)' \psi_k d\hat{s} - \\ - \sqrt{\beta} u \phi'_{n,1} \psi'_{m,1} \psi_{k,1}, \quad (\text{A.19})$$

for $k = 1, \dots, N_t$, $n = 1, \dots, N_a$ and $m = 1, \dots, N_t$,

$$\mathbf{V}^{(20)}(k, n, m) = \sqrt{\beta} u \int_0^1 \phi'_n \psi'_m \psi_k d\hat{s} + \sqrt{\beta} u \int_0^1 (\phi'_n \psi_m)' \psi_k d\hat{s} - \\ - \sqrt{\beta} u \phi'_{n,1} \psi_{m,1} \psi_{k,1}, \quad (\text{A.20})$$

for $k = 1, \dots, N_t$, $n = 1, \dots, N_a$ and $m = 1, \dots, N_t$,

$$\mathbf{V}^{(21)}(k, n, m) = \kappa_5 \int_0^1 (\psi'_n \Theta_m)' \psi_k d\hat{s} - \kappa_5 \psi'_{n,1} \Theta_{m,1} \psi_{k,1}, \quad (\text{A.21})$$

for $k = 1, \dots, N_t$, $n = 1, \dots, N_t$ and $m = 1, \dots, N_r$,

$$\begin{aligned}
\mathbf{V}^{(22)}(k, n, m, p) = & \frac{\kappa_2}{2} \int_0^1 (\psi'_n \psi'_m \psi'_p)' \psi_k d\hat{s} - 2 \int_0^1 (\psi'_n \psi''_m \psi''_p)' \psi_k d\hat{s} + \\
& + 2 \int_0^1 (\psi'_n \psi'_m \psi''_p)'' \psi_k d\hat{s} - \frac{\kappa_2}{2} \psi'_{n,1} \psi'_{m,1} \psi'_{p,1} \psi_{k,1} + 2 \psi'_{n,1} \psi''_{m,1} \psi''_{p,1} \psi_{k,1} - \\
& - 2 (\psi'_n \psi'_m \psi''_p)'|_{\hat{s}=1} \psi_{k,1} + \frac{u^2}{2} \psi'_{n,1} \psi'_{m,1} \psi'_{p,1} \psi_{k,1} + 2 \psi'_{n,1} \psi'_{m,1} \psi''_{p,1} \psi'_{k,1}, \quad (\text{A.22})
\end{aligned}$$

for $k = 1, \dots, N_t$, $n = 1, \dots, N_t$, $m = 1, \dots, N_t$ and $p = 1, \dots, N_t$,

$$\begin{aligned}
\mathbf{V}^{(23)}(k, n, m, p) = & \frac{\kappa_2}{2} \int_0^1 (\psi'_n \psi'_m \psi'_p)' \psi_k d\hat{s} - \int_0^1 (\psi'_n \psi''_m \psi''_p)' \psi_k d\hat{s} - \\
& - \int_0^1 (\psi''_n \psi'_m \psi''_p)' \psi_k d\hat{s} + \kappa_3 \int_0^1 (\psi'_n \psi''_m \psi''_p)' \psi_k d\hat{s} + \int_0^1 (\psi''_n \psi'_m \psi'_p)'' \psi_k d\hat{s} + \\
& + \int_0^1 (\psi'_n \psi'_m \psi''_p)'' \psi_k d\hat{s} - \frac{\kappa_2}{2} \psi'_{n,1} \psi'_{m,1} \psi'_{p,1} \psi_{k,1} + \psi'_{n,1} \psi''_{m,1} \psi''_{p,1} \psi_{k,1} + \\
& + \psi''_{n,1} \psi'_{m,1} \psi''_{p,1} \psi_{k,1} - \kappa_3 \psi'_{n,1} \psi''_{m,1} \psi''_{p,1} \psi_{k,1} - (\psi''_n \psi'_m \psi'_p)'|_{\hat{s}=1} \psi_{k,1} - \\
& - (\psi'_n \psi'_m \psi''_p)'|_{\hat{s}=1} \psi_{k,1} + \frac{u}{2} \psi'_{n,1} \psi'_{m,1} \psi'_{p,1} \psi_{k,1} + \psi''_{n,1} \psi'_{m,1} \psi'_{p,1} \psi'_{k,1} + \\
& + \psi'_{n,1} \psi'_{m,1} \psi''_{p,1} \psi'_{k,1}, \quad (\text{A.23})
\end{aligned}$$

for $k = 1, \dots, N_t$, $n = 1, \dots, N_t$, $m = 1, \dots, N_t$ and $p = 1, \dots, N_t$,

$$\mathbf{V}^{(24)}(k, n, m, p) = \frac{\kappa_1}{2} \int_0^1 (\psi'_n \Theta'_m \Theta'_p)' \psi_k d\hat{s} - \frac{\kappa_1}{2} \psi'_{n,1} \Theta'_{m,1} \Theta'_{p,1} \psi_{k,1}, \quad (\text{A.24})$$

for $k = 1, \dots, N_t$, $n = 1, \dots, N_t$, $m = 1, \dots, N_r$ and $p = 1, \dots, N_r$,

$$\begin{aligned}\mathbf{V}^{(25)}(k, n, m, p) = & \frac{3}{2}\sqrt{\beta}u\int_0^1\psi'_n\psi'_m\psi'_p\psi_kd\hat{s} + \frac{3}{2}\sqrt{\beta}u\int_0^1(\psi_n\psi'_m\psi'_p)''\psi_kd\hat{s} - \\ & - \frac{3}{2}\sqrt{\beta}u\psi_{n,1}\psi'_{m,1}\psi'_{p,1}\psi_{k,1},\end{aligned}\quad (\text{A.25})$$

for $k = 1, \dots, N_t$, $n = 1, \dots, N_t$, $m = 1, \dots, N_t$ and $p = 1, \dots, N_t$,

$$\begin{aligned}\mathbf{V}^{(26)}(k, n, m, p) = & \frac{1}{2}\sqrt{\beta}u\int_0^1\psi'_n\psi'_m\psi'_p\psi_kd\hat{s} + \frac{1}{2}\sqrt{\beta}u\int_0^1(\psi_n\psi'_m\psi'_p)''\psi_kd\hat{s} - \\ & - \frac{1}{2}\sqrt{\beta}u\psi_{n,1}\psi'_{m,1}\psi'_{p,1}\psi_{k,1},\end{aligned}\quad (\text{A.26})$$

for $k = 1, \dots, N_t$, $n = 1, \dots, N_t$, $m = 1, \dots, N_t$ and $p = 1, \dots, N_t$,

$$\begin{aligned}\mathbf{V}^{(27)}(k, n, m, p) = & \sqrt{\beta}u\int_0^1\psi'_n\psi'_m\psi'_p\psi_kd\hat{s} + \sqrt{\beta}u\int_0^1(\psi'_n\psi_m\psi'_p)''\psi_kd\hat{s} - \\ & - \sqrt{\beta}u\psi'_{n,1}\psi'_{m,1}\psi'_{p,1}\psi_{k,1},\end{aligned}\quad (\text{A.27})$$

for $k = 1, \dots, N_t$, $n = 1, \dots, N_t$, $m = 1, \dots, N_t$ and $p = 1, \dots, N_t$,

$$\mathbf{V}^{(28)}(k, n, m, p) = -\kappa_5\int_0^1(\psi'_n\psi'_m\psi'_p)''\psi_kd\hat{s} + \kappa_5\psi'_{n,1}\psi'_{m,1}\psi'_{p,1}\psi_{k,1}, \quad (\text{A.28})$$

for $k = 1, \dots, N_t$, $n = 1, \dots, N_t$, $m = 1, \dots, N_t$ and $p = 1, \dots, N_t$,

$$\mathbf{V}^{(29)}(k, n) = -\int_0^1\psi_n\psi_kd\hat{s}, \quad (\text{A.29})$$

for $k = 1, \dots, N_t$ and $n = 1, \dots, N_t$,

$$\begin{aligned}
\mathbf{V}^{(30)}(k, n) = & -2\sqrt{\beta}u \int_0^1 \psi'_n \psi_k d\hat{s} + \sqrt{\beta}u \int_0^1 \xi'_s \psi'_n \psi_k d\hat{s} + \\
& + \sqrt{\beta}u \int_0^1 (\xi'_s \psi_n)' \psi_k d\hat{s} - \sqrt{\beta}u \xi'_{s,1} \psi_{n,1} \psi_{k,1} - \sqrt{\beta}u \xi'_{s,\bar{\xi}_-} \psi_{n,\bar{\xi}_-} \psi_{k,\bar{\xi}_-} + \\
& + \sqrt{\beta}u \xi'_{s,\bar{\xi}_+} \psi_{n,\bar{\xi}_+} \psi_{k,\bar{\xi}_+}, \tag{A.30}
\end{aligned}$$

for $k = 1, \dots, N_t$ and $n = 1, \dots, N_t$,

$$\begin{aligned}
\mathbf{V}^{(31)}(k, n) = & \kappa_2 \int_0^1 (\xi'_s \psi'_n)' \psi_k d\hat{s} + \frac{\kappa_1}{2} \int_0^1 (\theta'^2_{x,s} \psi'_n)' \psi_k d\hat{s} - \\
& - \int_0^1 (\xi''_s \psi''_n)' \psi_k d\hat{s} - \int_0^1 \psi'''_n \psi_k d\hat{s} + \int_0^1 (\xi''_s \psi'_n)'' \psi_k d\hat{s} + 2 \int_0^1 (\xi'_s \psi''_n)'' \psi_k d\hat{s} - \\
& - \kappa_2 \xi'_{s,1} \psi'_{n,1} \psi_{k,1} - \frac{\kappa_1}{2} \theta'^2_{x,s,1} \psi'_{n,1} \psi_{k,1} + \xi''_{s,1} \psi''_{n,1} \psi_{k,1} + \psi'''_{n,1} \psi_{k,1} - \\
& - (\xi''_s \psi'_n)'|_{\hat{s}=1} \psi_{k,1} - u^2 \psi'_{n,1} \psi_{k,1} + u^2 \xi'_{s,1} \psi'_{n,1} \psi_{k,1} - 2(\xi'_s \psi''_n)'|_{\hat{s}=1} \psi_{k,1} - \\
& - \psi''_{n,1} \psi'_{k,1} + \xi''_{s,1} \psi'_{n,1} \psi'_{k,1} + 2\xi'_{s,1} \psi''_{n,1} \psi'_{k,1} - \kappa_2 \xi'_{s,\bar{\xi}_-} \psi'_{n,\bar{\xi}_-} \psi_{k,\bar{\xi}_-} + \\
& + \kappa_2 \xi'_{s,\bar{\xi}_+} \psi'_{n,\bar{\xi}_+} \psi_{k,\bar{\xi}_+} - \frac{\kappa_1}{2} \theta'^2_{x,s,\bar{\xi}_-} \psi'_{n,\bar{\xi}_-} \psi_{k,\bar{\xi}_-} + \frac{\kappa_1}{2} \theta'^2_{x,s,\bar{\xi}_+} \psi'_{n,\bar{\xi}_+} \psi_{k,\bar{\xi}_+} + \\
& + \xi''_{s,\bar{\xi}_-} \psi''_{n,\bar{\xi}_-} \psi_{k,\bar{\xi}_-} - \xi''_{s,\bar{\xi}_+} \psi''_{n,\bar{\xi}_+} \psi_{k,\bar{\xi}_+} - (\xi''_s \psi'_n)'|_{\hat{s}=\bar{\xi}_-} \psi_{k,\bar{\xi}_-} + \\
& + (\xi''_s \psi'_n)'|_{\hat{s}=\bar{\xi}_+} \psi_{k,\bar{\xi}_+} - 2(\xi'_s \psi''_n)'|_{\hat{s}=\bar{\xi}_-} \psi_{k,\bar{\xi}_-} + 2(\xi'_s \psi''_n)'|_{\hat{s}=\bar{\xi}_+} \psi_{k,\bar{\xi}_+} + \\
& + \xi''_{s,\bar{\xi}_-} \psi'_{n,\bar{\xi}_-} \psi'_{k,\bar{\xi}_-} - \xi''_{s,\bar{\xi}_+} \psi'_{n,\bar{\xi}_+} \psi'_{k,\bar{\xi}_+} + 2\xi'_{s,\bar{\xi}_-} \psi''_{n,\bar{\xi}_-} \psi'_{k,\bar{\xi}_-} - 2\xi'_{s,\bar{\xi}_+} \psi''_{n,\bar{\xi}_+} \psi'_{k,\bar{\xi}_+}, \tag{A.31}
\end{aligned}$$

for $k = 1, \dots, N_t$ and $n = 1, \dots, N_t$,

$$\begin{aligned}
\mathbf{V}^{(32)}(k, n) = & \kappa_3 \int_0^1 (\theta'_{x,s} \psi'_n)'' \psi_k d\hat{s} - \kappa_3 (\theta'_{x,s} \psi'_n)'|_{\hat{s}=1} \psi_{k,1} + \\
& + \kappa_3 \theta'_{x,s,1} \psi'_{n,1} \psi'_{k,1} - \kappa_3 (\theta'_{x,s} \psi'_n)'|_{\hat{s}=\bar{\xi}_-} \psi_{k,\bar{\xi}_-} + \kappa_3 (\theta'_{x,s} \psi'_n)'|_{\hat{s}=\bar{\xi}_+} \psi_{k,\bar{\xi}_+} + \\
& + \kappa_3 \theta'_{x,s,\bar{\xi}_-} \psi'_{n,\bar{\xi}_-} \psi'_{k,\bar{\xi}_-} - \kappa_3 \theta'_{x,s,\bar{\xi}_+} \psi'_{n,\bar{\xi}_+} \psi'_{k,\bar{\xi}_+}, \tag{A.32}
\end{aligned}$$

for $k = 1, \dots, N_t$ and $n = 1, \dots, N_t$,

$$\begin{aligned}
\mathbf{V}^{(33)}(k, n, m) = & \kappa_2 \int_0^1 (\phi'_n \psi'_m)' \psi_k d\hat{s} - \int_0^1 (\phi''_n \psi''_m)' \psi_k d\hat{s} + \\
& + \int_0^1 (\phi''_n \psi'_m)'' \psi_k d\hat{s} + 2 \int_0^1 (\phi'_n \psi''_m)'' \psi_k d\hat{s} - \kappa_2 \phi'_{n,1} \psi'_{m,1} \psi_{k,1} + \phi''_{n,1} \psi''_{m,1} \psi_{k,1} - \\
& - (\phi''_n \psi'_m)'|_{\hat{s}=1} \psi_{k,1} - 2 (\phi'_n \psi''_m)'|_{\hat{s}=1} \psi_{k,1} + u^2 \phi'_{n,1} \psi'_{m,1} \psi_{k,1} + \phi''_{n,1} \psi''_{m,1} \psi'_{k,1} + \\
& + 2 \phi'_{n,1} \psi''_{m,1} \psi'_{k,1}, \tag{A.33}
\end{aligned}$$

for $k = 1, \dots, N_t$, $n = 1, \dots, N_a$ and $m = 1, \dots, N_t$,

$$\begin{aligned}
\mathbf{V}^{(34)}(k, n, m) = & \kappa_1 \int_0^1 (\theta'_{x,s} \psi'_n \Theta'_m)' \psi_k d\hat{s} - \kappa_1 \theta'_{x,s,1} \psi'_{n,1} \Theta'_{m,1} \psi_{k,1} - \\
& - \kappa_1 \theta'_{x,s,\bar{\xi}_-} \psi'_{n,\bar{\xi}_-} \Theta'_{m,\bar{\xi}_-} \psi_{k,\bar{\xi}_-} + \kappa_1 \theta'_{x,s,\bar{\xi}_+} \psi'_{n,\bar{\xi}_+} \Theta'_{m,\bar{\xi}_+} \psi_{k,\bar{\xi}_+}, \tag{A.34}
\end{aligned}$$

for $k = 1, \dots, N_t$, $n = 1, \dots, N_t$ and $m = 1, \dots, N_r$,

$$\begin{aligned}
\mathbf{V}^{(35)}(k, n, m) = & \kappa_3 \int_0^1 (\psi'_n \Theta'_m)'' \psi_k d\hat{s} - \kappa_3 (\psi'_n \Theta'_m)'|_{\hat{s}=1} \psi_{k,1} + \\
& + \kappa_3 \psi'_{n,1} \Theta'_{m,1} \psi'_{k,1}, \tag{A.35}
\end{aligned}$$

for $k = 1, \dots, N_t$, $n = 1, \dots, N_t$ and $m = 1, \dots, N_r$,

$$\begin{aligned} \mathbf{V}^{(36)}(k, n, m) = & \sqrt{\beta} u \int_0^1 \phi'_n \psi'_m \psi_k d\hat{s} + \sqrt{\beta} u \int_0^1 (\phi'_n \psi'_m)' \psi_k d\hat{s} - \\ & - \sqrt{\beta} u \phi_{n,1} \psi'_{m,1} \psi_{k,1}, \end{aligned} \quad (\text{A.36})$$

for $k = 1, \dots, N_t$, $n = 1, \dots, N_a$ and $m = 1, \dots, N_t$,

$$\begin{aligned} \mathbf{V}^{(37)}(k, n, m) = & \sqrt{\beta} u \int_0^1 \phi'_n \psi'_m \psi_k d\hat{s} + \sqrt{\beta} u \int_0^1 (\phi'_n \psi'_m)' \psi_k d\hat{s} - \\ & - \sqrt{\beta} u \phi'_{n,1} \psi'_{m,1} \psi_{k,1}, \end{aligned} \quad (\text{A.37})$$

for $k = 1, \dots, N_t$, $n = 1, \dots, N_a$ and $m = 1, \dots, N_t$,

$$\mathbf{V}^{(38)}(k, n, m) = -\kappa_5 \int_0^1 (\psi'_n \Theta_m)' \psi_k d\hat{s} + \kappa_5 \psi'_{n,1} \Theta_{m,1} \psi_{k,1}, \quad (\text{A.38})$$

for $k = 1, \dots, N_t$, $n = 1, \dots, N_t$ and $m = 1, \dots, N_r$,

$$\mathbf{V}^{(39)}(k, n, m) = -\kappa_5 \int_0^1 (\psi'_n \Theta_m)' \psi_k d\hat{s} + \kappa_5 \psi'_{n,1} \Theta_{m,1} \psi_{k,1}, \quad (\text{A.39})$$

for $k = 1, \dots, N_t$, $n = 1, \dots, N_t$ and $m = 1, \dots, N_r$,

$$\begin{aligned} \mathbf{V}^{(40)}(k, n, m, p) = & \frac{\kappa_2}{2} \int_0^1 (\psi'_n \psi'_m \psi'_p)' \psi_k d\hat{s} - 2 \int_0^1 (\psi'_n \psi''_m \psi''_p)' \psi_k d\hat{s} + \\ & + 2 \int_0^1 (\psi'_n \psi'_m \psi''_p)'' \psi_k d\hat{s} - \frac{1}{2} \kappa_2 \psi'_{n,1} \psi'_{m,1} \psi'_{p,1} \psi_{k,1} + 2 \psi'_{n,1} \psi''_{m,1} \psi''_{p,1} \psi_{k,1} - \\ & - 2 (\psi'_n \psi'_m \psi''_p)'|_{\hat{s}=1} \psi_{k,1} + \frac{u^2}{2} \psi'_{n,1} \psi'_{m,1} \psi'_{p,1} \psi_{k,1} + 2 \psi'_{n,1} \psi'_{m,1} \psi''_{p,1} \psi'_{k,1}, \end{aligned} \quad (\text{A.40})$$

for $k = 1, \dots, N_t$, $n = 1, \dots, N_t$, $m = 1, \dots, N_t$ and $p = 1, \dots, N_t$,

$$\begin{aligned}
\mathbf{V}^{(41)}(k, n, m, p) = & \frac{\kappa_2}{2} \int_0^1 (\psi'_n \psi'_m \psi'_p)' \psi_k d\hat{s} - \int_0^1 (\psi''_n \psi''_m \psi''_p)' \psi_k d\hat{s} - \\
& - \int_0^1 (\psi'_n \psi''_m \psi''_p)' \psi_k d\hat{s} + \int_0^1 (\psi'_n \psi'_m \psi''_p)'' \psi_k d\hat{s} + \int_0^1 (\psi''_n \psi'_m \psi'_p)'' \psi_k d\hat{s} - \\
& - \kappa_3 \int_0^1 (\psi'_n \psi'_m \psi''_p)'' \psi_k d\hat{s} - \frac{1}{2} \kappa_2 \psi'_{n,1} \psi'_{m,1} \psi'_{p,1} \psi_{k,1} + \psi''_{n,1} \psi''_{m,1} \psi'_{p,1} \psi_{k,1} + \\
& + \psi'_{n,1} \psi''_{m,1} \psi''_{p,1} \psi_{k,1} - (\psi'_n \psi'_m \psi''_p)'|_{\hat{s}=1} \psi_{k,1} - (\psi''_n \psi''_m \psi''_p)'|_{\hat{s}=1} \psi_{k,1} + \\
& + \kappa_3 (\psi'_n \psi'_m \psi''_p)'|_{\hat{s}=1} \psi_{k,1} + \frac{u^2}{2} \psi'_{n,1} \psi'_{m,1} \psi'_{p,1} \psi_{k,1} + \psi'_{n,1} \psi'_{m,1} \psi''_{p,1} \psi'_{k,1} + \\
& + \psi''_{n,1} \psi'_{m,1} \psi'_{p,1} \psi'_{k,1} - \kappa_3 \psi'_{n,1} \psi'_{m,1} \psi''_{p,1} \psi'_{k,1}, \tag{A.41}
\end{aligned}$$

for $k = 1, \dots, N_t$, $n = 1, \dots, N_t$, $m = 1, \dots, N_t$ and $p = 1, \dots, N_t$,

$$\mathbf{V}^{(42)}(k, n, m, p) = \frac{\kappa_1}{2} \int_0^1 (\psi'_n \Theta'_m \Theta'_p)' \psi_k d\hat{s} - \frac{\kappa_1}{2} \psi'_{n,1} \Theta'_{m,1} \Theta'_{p,1} \psi_{k,1}, \tag{A.42}$$

for $k = 1, \dots, N_t$, $n = 1, \dots, N_t$, $m = 1, \dots, N_r$ and $p = 1, \dots, N_r$,

$$\begin{aligned}
\mathbf{V}^{(43)}(k, n, m, p) = & \frac{3}{2} \sqrt{\beta} u \int_0^1 \psi'_n \psi'_m \psi'_p \psi_k d\hat{s} + \frac{3}{2} \sqrt{\beta} u \int_0^1 (\psi_n \psi'_m \psi'_p)' \psi_k d\hat{s} - \\
& - \frac{3}{2} \sqrt{\beta} u \psi'_{n,1} \psi'_{m,1} \psi'_{p,1} \psi_{k,1}, \tag{A.43}
\end{aligned}$$

for $k = 1, \dots, N_t$, $n = 1, \dots, N_t$, $m = 1, \dots, N_t$ and $p = 1, \dots, N_t$,

$$\begin{aligned}
\mathbf{V}^{(44)}(k, n, m, p) = & \frac{1}{2} \sqrt{\beta} u \int_0^1 \psi'_n \psi'_m \psi'_p \psi_k d\hat{s} + \frac{1}{2} \sqrt{\beta} u \int_0^1 (\psi'_n \psi'_m \psi'_p)' \psi_k d\hat{s} - \\
& - \frac{1}{2} \sqrt{\beta} u \psi'_{n,1} \psi'_{m,1} \psi'_{p,1} \psi_{k,1}, \tag{A.44}
\end{aligned}$$

for $k = 1, \dots, N_t$, $n = 1, \dots, N_t$, $m = 1, \dots, N_t$ and $p = 1, \dots, N_t$,

$$\begin{aligned} \mathbf{V}^{(45)}(k, n, m, p) &= \sqrt{\beta} u \int_0^1 \psi'_n \psi'_m \psi'_p \psi_k d\hat{s} + \sqrt{\beta} u \int_0^1 (\psi'_n \psi_m \psi'_p)' \psi_k d\hat{s} - \\ &- \sqrt{\beta} u \psi'_{n,1} \psi_{m,1} \psi'_{p,1} \psi_{k,1}, \end{aligned} \quad (\text{A.45})$$

for $k = 1, \dots, N_t$, $n = 1, \dots, N_t$, $m = 1, \dots, N_t$ and $p = 1, \dots, N_t$,

$$\mathbf{V}^{(46)}(k, n, m, p) = 2\kappa_5 \int_0^1 (\psi'_n \psi'_m \psi'_p)' \psi_k d\hat{s} - 2\kappa_5 \psi'_{n,1} \psi'_{m,1} \psi'_{p,1} \psi_{k,1}, \quad (\text{A.46})$$

for $k = 1, \dots, N_t$, $n = 1, \dots, N_t$, $m = 1, \dots, N_t$ and $p = 1, \dots, N_t$,

$$\mathbf{V}^{(47)}(k, n, m, p) = \kappa_5 \int_0^1 (\psi'_n \psi'_m \psi'_p)' \psi_k d\hat{s} - \kappa_5 \psi'_{n,1} \psi'_{m,1} \psi'_{p,1} \psi_{k,1}, \quad (\text{A.47})$$

for $k = 1, \dots, N_t$, $n = 1, \dots, N_t$, $m = 1, \dots, N_t$ and $p = 1, \dots, N_t$,

$$\mathbf{V}^{(49)}(k, n) = -\kappa_5 \int_0^1 \Theta_n \Theta_k d\hat{s}, \quad (\text{A.48})$$

for $k = 1, \dots, N_r$ and $n = 1, \dots, N_r$,

$$\begin{aligned} \mathbf{V}^{(51)}(k, n) &= \kappa_1 \int_0^1 (\xi'_s \Theta'_n)' \Theta_k d\hat{s} + \frac{3}{2} \kappa_4 \int_0^1 (\theta'^2_{x,s} \Theta'_n)' \Theta_k d\hat{s} + \kappa_3 \int_0^1 \Theta''_n \Theta_k d\hat{s} - \\ &- \kappa_1 \xi'_{s,1} \Theta'_{n,1} \Theta_{k,1} - \frac{3}{2} \kappa_4 \theta'^2_{x,s,1} \Theta'_{n,1} \Theta_{k,1} - \kappa_3 \Theta'_{n,1} \Theta_{k,1} - \kappa_1 \xi'_{s,\bar{\xi}_-} \Theta'_{n,\bar{\xi}_-} \Theta_{k,\bar{\xi}_-} + \\ &+ \kappa_1 \xi'_{s,\bar{\xi}_+} \Theta'_{n,\bar{\xi}_+} \Theta_{k,\bar{\xi}_+} - \frac{3}{2} \kappa_4 \theta'^2_{x,s,\bar{\xi}_-} \Theta'_{n,\bar{\xi}_-} \Theta_{k,\bar{\xi}_-} + \frac{3}{2} \kappa_4 \theta'^2_{x,s,\bar{\xi}_+} \Theta'_{n,\bar{\xi}_+} \Theta_{k,\bar{\xi}_+}, \end{aligned} \quad (\text{A.49})$$

for $k = 1, \dots, N_r$ and $n = 1, \dots, N_r$,

$$\begin{aligned} \mathbf{V}^{(52)}(k, n) = & \kappa_1 \int_0^1 (\phi'_n \theta'_{x,s})' \Theta_k d\hat{s} - \kappa_1 \phi'_{n,1} \theta'_{x,s,1} \Theta_{k,1} - \\ & - \kappa_1 \phi'_{n,\bar{\xi}_-} \theta'_{x,s,\bar{\xi}_-} \Theta_{k,\bar{\xi}_-} + \kappa_1 \phi'_{n,\bar{\xi}_+} \theta'_{x,s,\bar{\xi}_+} \Theta_{k,\bar{\xi}_+}, \end{aligned} \quad (\text{A.50})$$

for $k = 1, \dots, N_r$ and $n = 1, \dots, N_a$,

$$\begin{aligned} \mathbf{V}^{(53)}(k, n, m) = & \frac{3}{2} \kappa_4 \int_0^1 (\theta'_{x,s} \Theta'_n \Theta'_m)' \Theta_k d\hat{s} - \frac{3}{2} \kappa_4 \theta'_{x,s,1} \Theta'_{n,1} \Theta'_{m,1} \Theta_{k,1} - \\ & - \frac{3}{2} \kappa_4 \theta'_{x,s,\bar{\xi}_-} \Theta'_{n,\bar{\xi}_-} \Theta'_{m,\bar{\xi}_-} \Theta_{k,\bar{\xi}_-} + \frac{3}{2} \kappa_4 \theta'_{x,s,\bar{\xi}_+} \Theta'_{n,\bar{\xi}_+} \Theta'_{m,\bar{\xi}_+} \Theta_{k,\bar{\xi}_+}, \end{aligned} \quad (\text{A.51})$$

for $k = 1, \dots, N_r$, $n = 1, \dots, N_r$ and $m = 1, \dots, N_r$,

$$\mathbf{V}^{(54)}(k, n, m) = \kappa_1 \int_0^1 (\phi'_n \Theta'_m)' \Theta_k d\hat{s} - \kappa_1 \phi'_{n,1} \Theta'_{m,1} \Theta_{k,1}, \quad (\text{A.52})$$

for $k = 1, \dots, N_r$, $n = 1, \dots, N_a$ and $m = 1, \dots, N_r$,

$$\begin{aligned} \mathbf{V}^{(55)}(k, n, m) = & \frac{1}{2} \kappa_1 \int_0^1 (\psi'_n \psi'_m \theta'_{x,s})' \Theta_k d\hat{s} - \frac{1}{2} \kappa_1 \psi'_{n,1} \psi'_{m,1} \theta'_{x,s,1} \Theta_{k,1} - \\ & - \frac{1}{2} \kappa_1 \psi'_{n,\bar{\xi}_-} \psi'_{m,\bar{\xi}_-} \theta'_{x,s,\bar{\xi}_-} \Theta_{k,\bar{\xi}_-} + \frac{1}{2} \kappa_1 \psi'_{n,\bar{\xi}_+} \psi'_{m,\bar{\xi}_+} \theta'_{x,s,\bar{\xi}_+} \Theta_{k,\bar{\xi}_+}, \end{aligned} \quad (\text{A.53})$$

for $k = 1, \dots, N_r$, $n = 1, \dots, N_t$ and $m = 1, \dots, N_t$,

$$\begin{aligned} \mathbf{V}^{(56)}(k, n, m) = & \frac{1}{2} \kappa_1 \int_0^1 (\psi'_n \psi'_m \theta'_{x,s})' \Theta_k d\hat{s} - \frac{1}{2} \kappa_1 \psi'_{n,1} \psi'_{m,1} \theta'_{x,s,1} \Theta_k - \\ & - \frac{1}{2} \kappa_1 \psi'_{n,\bar{\xi}_-} \psi'_{m,\bar{\xi}_-} \theta'_{x,s,\bar{\xi}_-} \Theta_k + \frac{1}{2} \kappa_1 \psi'_{n,\bar{\xi}_+} \psi'_{m,\bar{\xi}_+} \theta'_{x,s,\bar{\xi}_+} \Theta_k, \end{aligned} \quad (\text{A.54})$$

for $k = 1, \dots, N_r$, $n = 1, \dots, N_t$ and $m = 1, \dots, N_t$,

$$\mathbf{V}^{(57)}(k, n, m) = -\kappa_3 \int_0^1 (\psi'_n \psi''_m)' \Theta_k d\hat{s} + \kappa_3 \psi'_{n,1} \psi''_{m,1} \Theta_{k,1}, \quad (\text{A.55})$$

for $k = 1, \dots, N_r$, $n = 1, \dots, N_t$ and $m = 1, \dots, N_t$,

$$\mathbf{V}^{(58)}(k, n, m) = \kappa_5 \int_0^1 \psi'_n \psi'_m \Theta_k d\hat{s}, \quad (\text{A.56})$$

for $k = 1, \dots, N_r$, $n = 1, \dots, N_t$ and $m = 1, \dots, N_t$,

$$\mathbf{V}^{(59)}(k, n, m) = \kappa_5 \int_0^1 \psi'_n \psi'_m \Theta_k d\hat{s}, \quad (\text{A.57})$$

for $k = 1, \dots, N_r$, $n = 1, \dots, N_t$ and $m = 1, \dots, N_t$,

$$\mathbf{V}^{(60)}(k, n, m, p) = \frac{1}{2} \kappa_4 \int_0^1 (\Theta'_n \Theta'_m \Theta'_p)' \Theta_k d\hat{s} - \frac{1}{2} \kappa_4 \Theta'_{n,1} \Theta'_{m,1} \Theta'_{p,1} \Theta_{k,1}, \quad (\text{A.58})$$

for $k = 1, \dots, N_r$, $n = 1, \dots, N_r$, $m = 1, \dots, N_r$ and $p = 1, \dots, N_r$,

$$\mathbf{V}^{(61)}(k, n, m, p) = \frac{1}{2} \kappa_1 \int_0^1 (\psi'_n \psi'_m \Theta'_p)' \Theta_k d\hat{s} - \frac{1}{2} \kappa_1 \psi'_{n,1} \psi'_{m,1} \Theta'_{p,1} \Theta_{k,1}, \quad (\text{A.59})$$

for $k = 1, \dots, N_r$, $n = 1, \dots, N_t$, $m = 1, \dots, N_t$ and $p = 1, \dots, N_r$,

$$\mathbf{V}^{(62)}(k, n, m, p) = \frac{1}{2} \kappa_1 \int_0^1 (\psi'_n \psi'_m \Theta'_p)' \Theta_k d\hat{s} - \frac{1}{2} \kappa_1 \psi'_{n,1} \psi'_{m,1} \Theta'_{p,1} \Theta_{k,1}, \quad (\text{A.60})$$

for $k = 1, \dots, N_r$, $n = 1, \dots, N_t$, $m = 1, \dots, N_t$ and $p = 1, \dots, N_r$.